R S Morrison Honours thesis

Supervisor: J D Foden

THE GEOLOGY, PETROLOGY AND GEOCHEMISTRY OF SOUTHWEST SAINT FRANCIS ISLAND, SOUTH AUSTRALIA.

THE UNIVERSITY OF ADELAIDE

SCHOOL OF GEOLOGY

HONOURS 1982

This thesis may be lent or photocopied after a period of 0 * months from the date of sumbission.

Signature:.....R.S. Morrison.....

(* twelve months maximum permitted).

Frontispiece.

Southern coast of Saint Francis Island.

Abstract

The geology of Saint Francis Island, South Australia, consists of two separate crystalline basement complexes: the acid volcanic complex to the northwest and the slightly younger alkali granite complex to the south. The acid volcanic complex, composed of mainly tuffaceous rhyolite, is intruded by contemporanous dacite dykes and later by a leucogranite plug. The alkali granite is host to a set of rhyolite dykes and one megacrystic dacite porphyry dyke. The crystalline basement complexes have been correlated to the middle Proterozoic Gawler Range volcano-plutonic complex of South Australia.

Magma parental to the acid volcanic suite developed by means of crystal fractionation of more basic material at lower continental crustal regions. Intrusion of hot lower crustal melt into shallow crustal levels caused partial eutectic melting and the development of an alkali granite pluton which intruded the acid volcanic pile.

Table of Contents

List of Maps, Tables, Plates and Figures.

Maps.

Tables.

Plates.

Figures.

1. Introduction.

This thesis is an account of a detailed geological investigation into the crystalline basement rocks exposed on the southwest coast of Saint Francis Island, South Australia. This was accomplished at the University of Adelaide by geochemical and petrological examination of collected rock samples from the various lithologies encountered. Fieldwork was completed in collaboration with the Department of Mines and Energy of South Australia as part of a regional geological survey of the Nuyts Archipelago.

1.1 Location.

Saint Francis Island, the largest island of the Nuyts Archipelago, is located sixty-five kilometers southwest of Ceduna, South Australia (Map 1). The island itself is approximately four kilometers long, two kilometers wide and has a coastline in excess of seventeen kilometers.

1.2 Purpose of study.

The intention of this geological examination is not only to determine lithological relationships of the crystalline basement of Saint Francis Island by means of detailed mapping, but also through intensive geochemical and petrological study, to correlate the rocks within known stratigraphy of South Australia and to propose and evaluate an applicable scheme for its petrogenesis.

1.3 Previous work.

After the European discovery of Saint Francis Island by the Dutch in 1627, Walker and Botham in 1968, and later Kinsman in 1973, were the first to examine the geology of Saint Francis Island by interpreting aerial photographs. R.B. Major from the Department of Mines and Energy of South Australia visited the island in 1973 and collected a few samples. Flint and Crooks visited the island in 1981 for the Department of Mines and Energy, however no detailed metholodical mapping of the geology has ever been accomplished prior to this study.

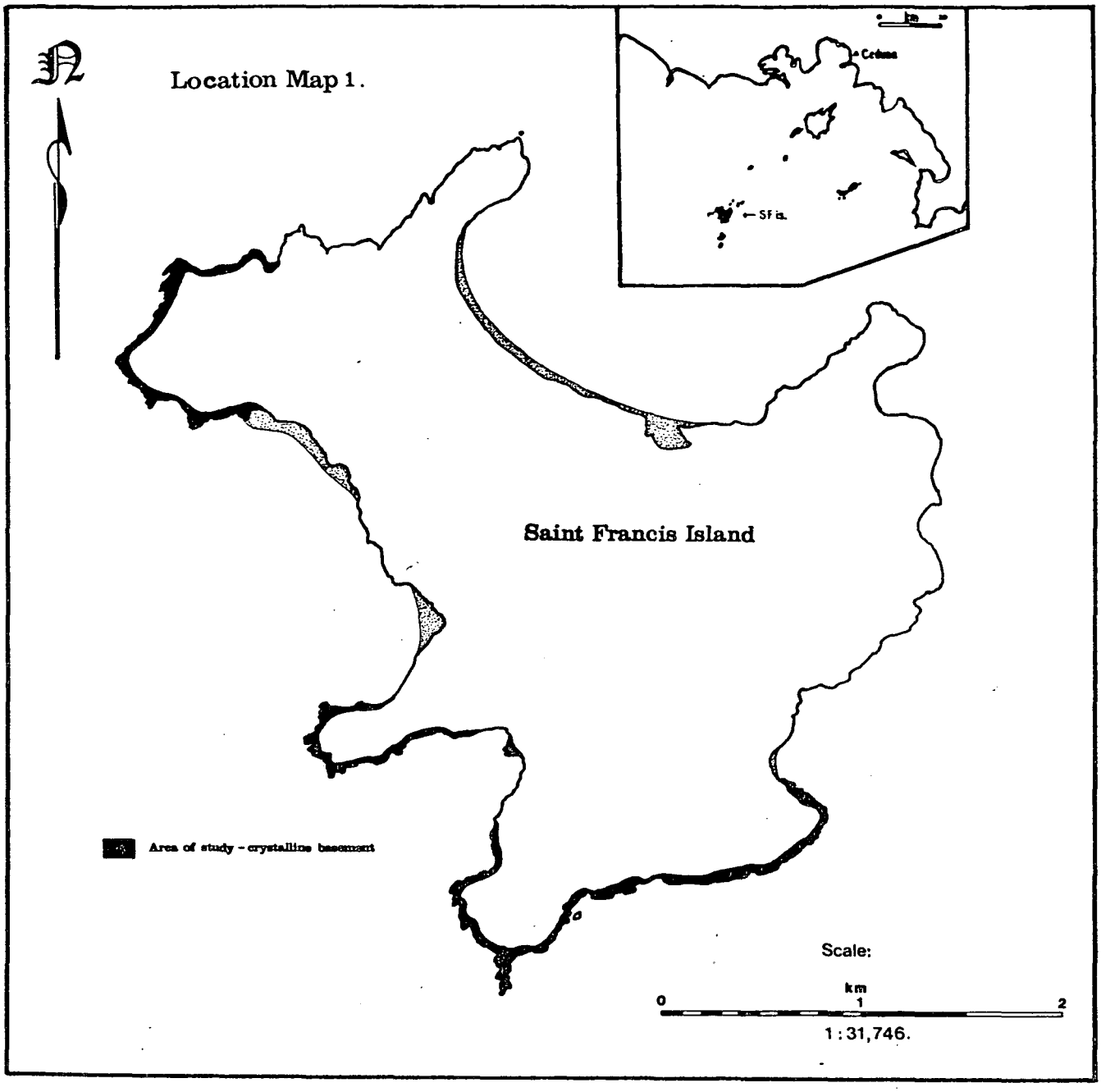
N
Location Map 1.
Cebu
SFis.
Saint Francis Island
Area of study - crystalline basement
Scale:
km
0
1
2
1:31,746.

In February, 1982, an expedition from the Department of Mines and Energy, including the author and C. Rosier from the University of Adelaide, mapped the islands of the Nuyts Archipelago. The data collected from this expedition are to be found in government reports to be published, and in two Honours theses from the University of Adelaide of which this is one.

1.4 Classification of lithologies.

The classification scheme of O'Connor (1965) with the igneous rocks of Saint Francis Island is shown in figure 1. However, for simplicity in this study, all fine grained rocks with weight SiO_2 greater than70% are termed 'rhyolite' and those rocks with SiO_2 less than 70% are called 'dacite'. The term 'alkali granite' was first used by Flint and Crooks (op.cit.) and is retained in this thesis. 'Leucogranite' refers to a pink granite plug. The prefix 'leuco' is used to distinguish it from the alkali granite.

2. Geology - Field Relations.

2.1 Introduction.

The crystalline basement rocks of Saint Francis Island can be grouped into two major complexes;

1. the acid volcanic complex to the northwest and
2. the alkali granite complex to the southeast (Map 2). The contact between these two complexes is covered by beach sand and Pleistocene sediment of the Bridgewater Formation.

The acid volcanic complex consists mainly of dark green to red porphyritic rhyolite which is intruded by two black porphyritic dacite dykes and one leucogranite plug with associated radiating felsic dykes. The alkali granite is composed of a large alkali granite pluton which itself is intruded by a megacrystic dacite porphyry dyke and a set of three red rhyolite dykes. These intrusions appear to be independent of the porphyritic acid volcanics due to the fine grained texture and high siliceous content of the rhyolite dykes and the coarsely porphyritic nature of the dacite porphyry. Both

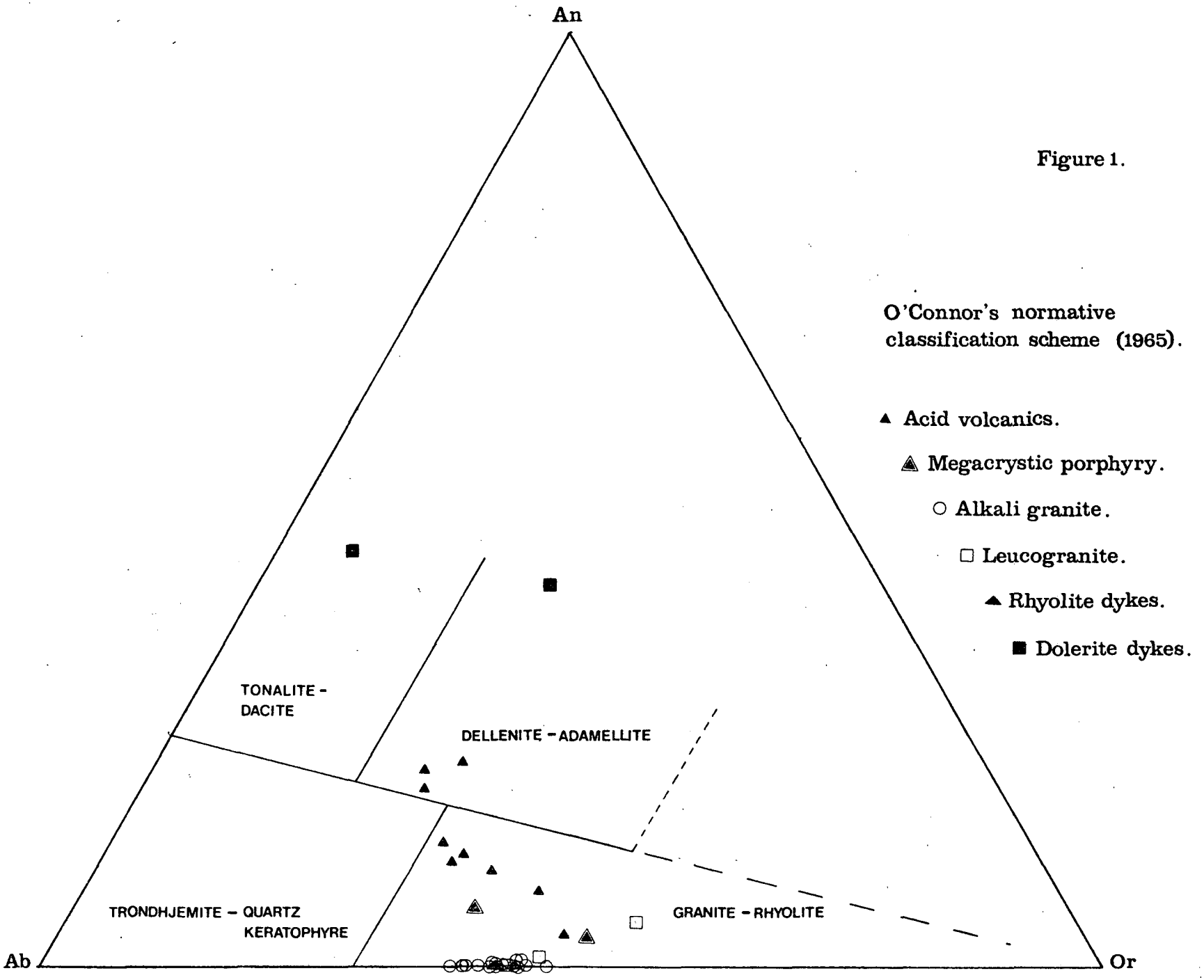

Figure 1.

O'Connor's normative classification scheme (1965).

▲ Acid volcanics.

▲ Megacrystic porphyry.

○ Alkali granite.

□ Leucogranite.

▲ Rhyolite dykes.

■ Dolerite dykes.

Geology of Southwest Saint Francis Island, South Australia.

SCALE 1 : 15,748.

0 — 0.5 — 1

km

Reference:

Cainozoic — Q — Bridgewater Formation.

Palaeozoic (?) — D — Dolerite.

Mid Proterozoic

- Ax — Rhyolite dykes.
- Ay — Megacrystic dacite porphyry. — Alkali granite complex.
- Az — Alkali granite.
- Ba — Leucogranite.
- Bb — Dacite. — Acid volcanic complex.
- Bc — Rhyolite.

Quartz shear zone.

Contact known, assumed.

Beach sand.

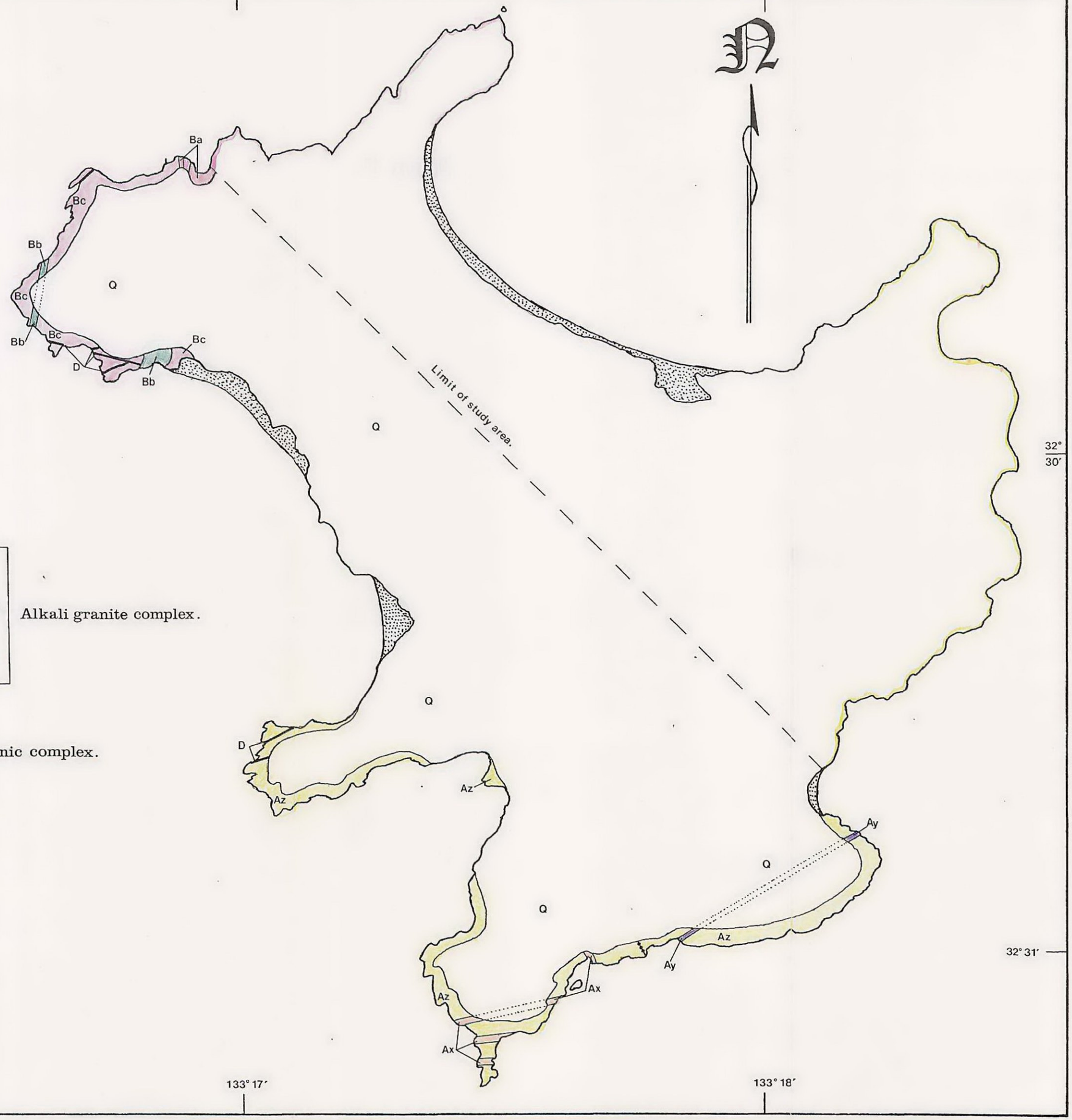

complexes have been intruded by a set of near vertical dolerite dykes which in turn have been intruded by aplite dykes.

2.2 Acid volcanic complex.

The dominant lithology of the acid volcanic complex is a homogeneous porphyritic rhyolite containing ten to twenty percent alkali feldspar and quartz phenocrysts 3-5 mm in diameter in a siliceous aphanitic groundmass. The rhyolite has two distinctive colours, dark green and red varieties (plate 1). The red colouration was found to be due to more advanced alteration in more highly fractured areas. Chlorite-carbonate-epidote veining through the rhyolite followed the regional trend of 20^{o}-50^{o} and there was no evidence of bedding or other primary sedimentary features. Small, elliptical breccia zones occur along quartz veins in the rhyolite (plate 2). These are believed to be in situ autobreccia caused by the escape of volatiles from the volcanic pile (Giles, 1981).

Intruding the rhyolite are two porphyritic dacite dykes five to ten metres wide with twenty percent quartz, alkali feldspar and plagioclase phenocrysts (5 mm in diameter) in a black aphanitic siliceous groundmass. The dykes come into sharp contact with little, if any, contact metamorphic effect of the host rhyolite. Although these dykes are generally linear, they have very irregularly shaped margins and may represent a contemporaneous volcanic event.

On the northern limit of the study area intrudes an equigranular quartz-feldspar leucogranite plug. Felsic dykes radiate from the leucogranite body, some of which display prominent flow landing. However, unlike the dacite dykes, the leucogranite dykes which intrude the acid volcanics are straight tabular bodies (plate 3).

2.3 Alkali granite complex.

The dominant lithology of the southwest coast is an equigranular medium grained quartz, alkali feldspar and plagioclase white alkali granite. Towards the margin of the granite body in the northwest, it becomes

Plate 1.

More highly fractured red porphyritic rhyolite (straddling hammer) between dark green porphyritic rhyolite in the acid volcanic complex.

Plate 2.

Insitu autobreccia within porphyritic rhyolite of the acid volcanic complex. Note epidote-chlorite-carbonate veining.


OLYMPUS

Plate 3.
Radiating felsic dyke
from leucogranite plug intruding acid volcanics.

Plate 4.
Quartz shear zone through alkali granite.
Note hat for scale.

increasingly porphyritic with medium grained phenocrysts in a fine grained groundmass. Quartz veining follows the regional trend of 20^{o}-50^{o}, and a quartz shear zone three metres wide and trending east-west cuts the granite (plate 4).

A set of three near vertical rhyolite dykes twenty metres wide and trending east-west intrude the southern-most exposure of the alkali granite. These quartz-alkali feldspars dykes often have a medium grained core grading to fine grained flow banded margins with abundant quartz veining along the contacts (plate 5).

These dykes appear to be a different lithology to the rhyolites of the acid volcanic complex due to their lack of phenocrysts and abundant quartz content.

To the east intrudes an eight metre wide megacrystic dacite porphyry dyke trending north-south. It consists of euhedral magacrysts of alkali feldspar in an aphanitic red groundmass (plate 6). There is little contact metamorphic effect on the host granite and no banded margins although a prominent schistosity is present in the dyke parallel to its margins.

2.4 Dolerite Dykes.

Through both the alkali granite complex and the acid volcanic complex occurs a set a subvertical dolerite dykes ranging from 0.2 m to 3 m in width and crosscutting all lithologies noted except for the rhyolite dykes of the alkali granite complex. Examination of the orientation of the dykes with respect to the jointing pattern of the host rocks shows clearly that the dykes tend to intrude along fractures (figures 2, 3). The higher concentration of dolerite dykes noted in the acid volcanics relative to the alkali granite is due to preferential intrusion into the more highly fractured acid volcanic complex (Price, 1966) (plate 7). In one location an aplite dyke 0.25m wide intruded into a dolerite dyke (plate 8).

2.5 Intrusive relations.

The nature of the dacite intrusions into host rhyolite of the acid

Plate 5.

Contact between alkali granite and a red rhyolite dyke.
Note abundant quartz veining.

Plate 6.

Contact between alkali granite and megacrystic dacite porphyry dyke.
Note schistosity in dyke.


OLYMPUS

Plate 7.
Dolerite dyke intruding acid volcanics.
Dyke is approximately one metre wide.

Plate 8.
Aplite dyke intruding dolerite dyke in acid volcanic complex.
Trend of dolerite dyke is indicated by hammer.

Figures 2 and 3.

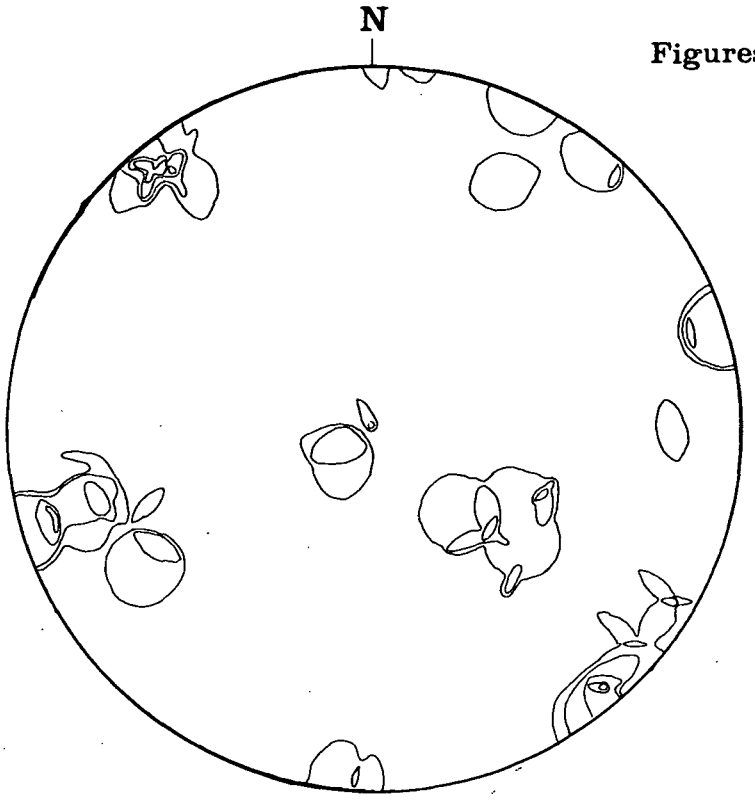

Stereonet of joint pattern. Contours show relative concentrations.

89 measurements.

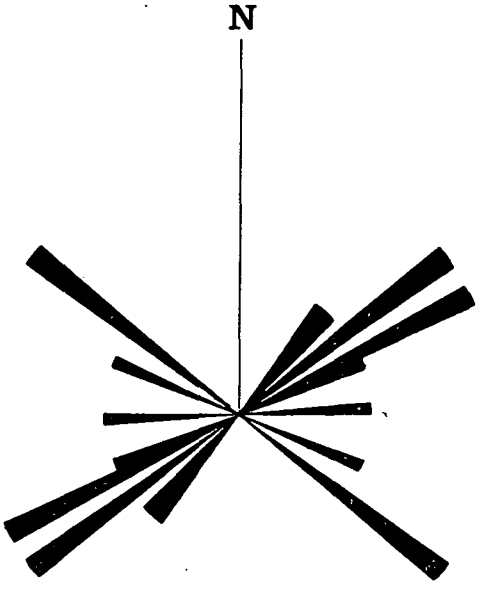

Rose diagram of dolerite dyke orientations.

11 measurements.

Figure 4.

Diagrammatic representation of intrusive relations.

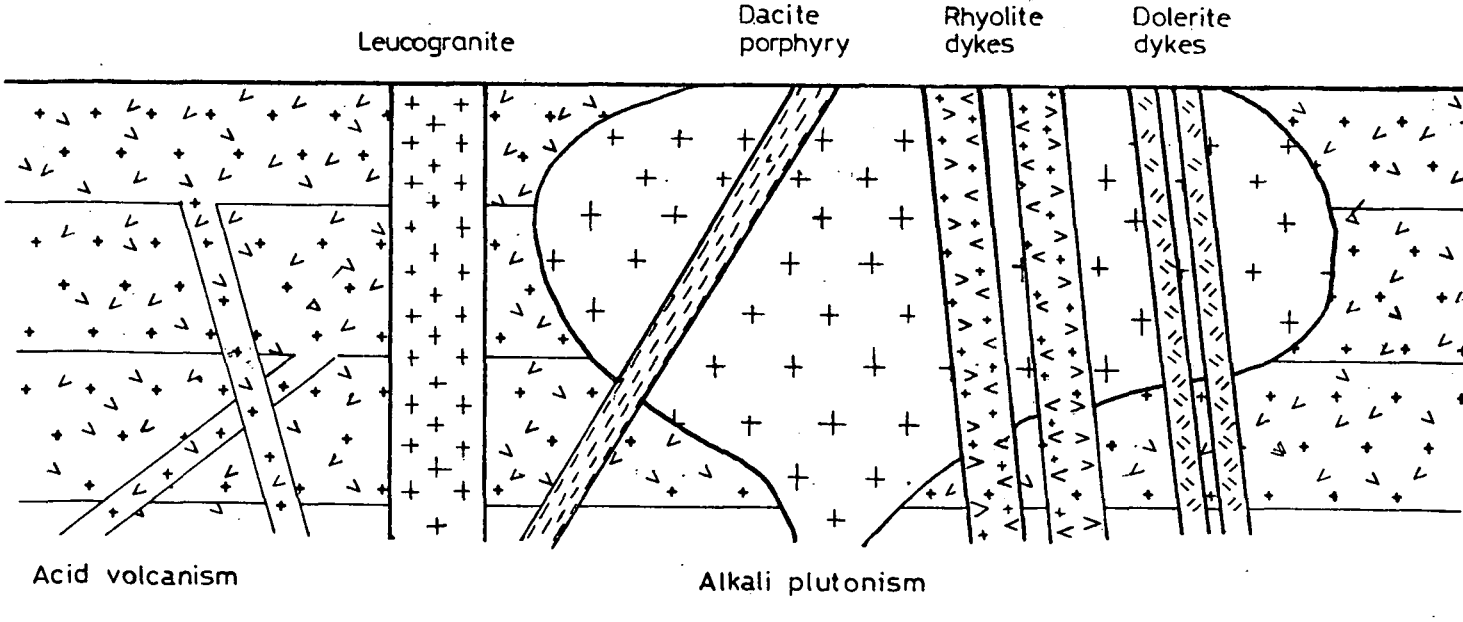

No scale intended.

volcanic complex suggests that both are contemporaneous volcanic events. Intrusion of the leucogranite plug into the acid volcanic pile would be followed by dolerite dyking and aplite dyking respectively. In the alkali granite complex, field evidence alone cannot adequately interpret the relative ages of intrusive emplacement and observation of the contact between the acid volcanic and alkali granite complexes was impossible due to cover. However, if the intensity of fracturing is indicative of relative age such that the older rocks are more highly fractured than younger ones, and assuming that the concentration of cooling joints is similar between the acid volcanics and the alkali granite, then it can be said that the acid volcanics represent the oldest rocks of the island into which were intruded the alkali granite. The intrusive relationships are summarised in figure 4.

3. Mineralogy and Petrography.

3.1 Introduction.

Fifty thin sections were examined from selected rocks collected: twelve from rhyolites and dacites of the acid volcanic complex (01-08, 12, 13, 25, 27), three from the leucogranite (9-11), four from the rhyolite dykes (15, 38D, 38F, 38J), two from the megacrystic dacite porphyry (17,23), two from the dolerite dykes (31,36) and twenty-seven from the alkali granite (14,18-22, 24, 28-30, 32-38C, 38E, 38G-I). The following is a synthesis of the mineralogy and petrography of the lithologies. Further description of representative samples can be found in Appendix IV.

3.2 Acid volcanic complex.

i. Porphyritic rhyolite and dacite.

The porphyritic rhyolite, a massive and homogeneous rock, is composed of ten to twenty percent phenocrysts of orthoclase, plagioclase and quartz in an orthophyric to felsophyric groundmass of quartz and alkali feldspar (plate 9). The euhedral Na-rich or K-rich feldspar phenocrysts range from 1-3 mm in diameter and often occur as shattered, angular crystals.

The alkali feldspars show microperthitic intergrowths of albite to varying degrees. Albite plagioclase occurs as individual crystals 1 mm in diameter or as larger glomerophyric masses. There is no indication of compositional zonation within individual feldspar grains, nor is there variation within the entire lithology. Quartz phenocrysts present fifteen to twenty percent of the total phenocryst content of the rock. The larger phenocrysts are embayed, partially rounded or eroded, and display undulose extinction. Smaller grains are angular and have uniform extinction. The groundmass consists of an intimate mosaic of quartz and alkali feldspar, the grain size of which varies between samples. Biotite and epidote are the main mafic constituents, the former being effected by chlorite and carbonate alteration. Interstitial haematite occurs in places and the feldspar grains have been sericitized. Accessory minerals include zircon and apatite which occur as pseudomorphs after mafic minerals and as small individual crystals in the groundmass.

The dacites differ slightly from the rhyolites in having a higher content of coarser feldspar phenocrysts. One of the dacites (05) displays prominent spherulites of finely fibrous alkali feldspar crystallites often radiating from quartz phenocrysts.

The acid volcanic rhyolites and dacites are crystal tuffs with intratelluric feldspars and quartz phenocrysts. Differences in groundmass textures suggest that variations may be dependent on depth of tuff sheet (Turner, 1975).

ii. Leucogranite.

The leucogranite is a holocrystalline hypidiomorphic granular quartz-feldspar granite. Feldspars consist of up to twenty percent albite plagioclase and fifty percent orthoclase, some of which has microperthitic texture. Quartz, which occurs as anhedral grains with undulose extinction, is often graphically intergrown with orthoclase.

Alteration occurs as interstitial haematite and sericitization of feldspars.

3.3 Alkali Granite Complex.

i. Alkali granite.

The alkali granite has a hypidiomorphic holocrystalline quartz-feldspar texture on the east coast of Saint Francis Island and grades to a quartz-feldspar porphyry towards the west.

The felspars consist of microcline, some of which has been altered to orthoclase and albite. The albite content is approximately ten percent of the rock volume and exists as small individual grains or as microperthitic intergrowths with alkali feldspar. Quartz is graphically intergrown with alkali feldspar, and in some samples, boundaries between quartz and alkali feldspar display myrmekitic exsolution texture (plate 10). In the porphyritic western area of the alkali granite, quartz occurs as euhedral phenocrysts in a quartz-feldspar groundmass.

Mafic minerals include clinopyroxene, epidote and magnetite. Zircon occurs as euhedral crystals within magnetite or as glomerophyric xenocrysts. Alteration of the granite had developed interstitial haematite and carbonate with varying degrees of sericitization of the feldspars.

ii. Rhyolite dykes.

These dykes consist of quartz, orthoclase and minor albite which are intimately intergrown to form prominent graphic texture. Two samples (38J, 38D) have phenocrysts of quartz and orthoclase in a strongly spherulitic or graphic groundmass. Myrmekitic feldspars are present in other samples (38F, 15).

Mafic minerals include epidote, magnetite and interstitial biotite and haematite, but are a minor component. The dykes are relatively unaltered compared to the host alkali granite.

iii. Megacrystic dacite porphyry.

The megacrystic dacite porphyry dyke consists of rounded euhedral phenocrysts of orthoclase 5-10 mm in diameter. Minor albite accompanies the orthoclase in a fine grained orthophyric groundmass which shows microflow texture around phenocrysts (plate 11). Minor mafic minerals include biotite, magnetite and chlorite, and alteration has caused chloritization of biotite and sericitization of feldspars.

Plate 9.
Shattered fragments of orthoclase, quartz and albite in a felsophyric groundmass. Rhyolite tuff, sample 01.
Field of view is 7.5 mm, crossed polars.

Plate 10.
Graphically intergrown quartz and alkali feldspar with clinopyroxene (aegirine). Alkali granite, sample 21.
Field of view is 7.5 mm, crossed polars.

Plate 11.
Euhedral megacrysts of orthoclase in a felsophyric groundmass displaying flow texture. Megacrystic dacite porphyry, sample 23.
Field of view is 7.5 mm, crossed polars.

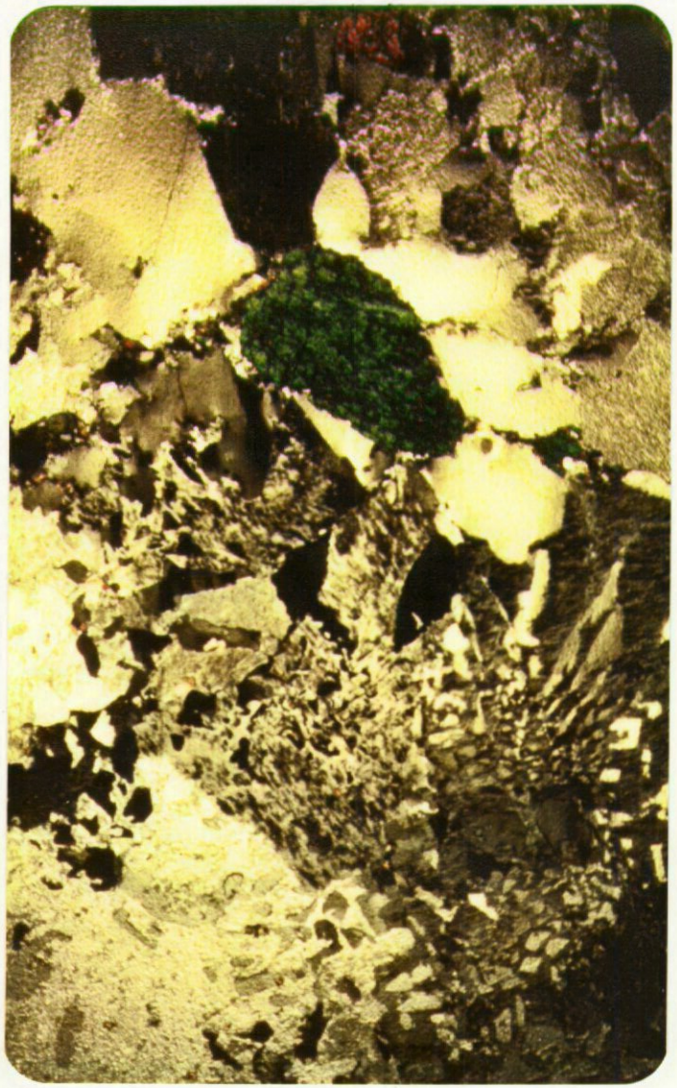

3.4 Dolerite.

The dolerite dykes are composed of mainly epidote and plagioclase. Plagioclase laths have grown into epidote forming ophitic texture. In sample 31, epidote occurs as glomerophyric phenocrysts although it usually exists as individual equigranular crystals.

4. Geochemistry.

4.1 Introduction.

Forty-five rocks were analysed for major oxide compositions expressed as weight percentages of SiO_2, Al_2O_3, MgO, MnO, CaO, Na_2O, K_2O, TiO_2 and P_2O_5. Iron was first calculated as total Fe_2O_3 and then divided into an appropriate FeO component. Accompanying major oxide analyses were measurements accomplished for trace element concentrations of Ba, Rb, Sr, Zr, Nd, Nb, Sc, V, Ni, Ce and Y. Appendix I records all results obtained. For two rocks, alkali granite 38I and acid volcanic 06, rare earth element contents were determined (Ce, Nd, Sm, Eu, Gd, Er and Yb). Analytical procedures for these analyses can be found in Appendix V.

4.2 Major oxide chemistry.

With the exception of the dolerite dykes (28,31) all rocks analysed have similar alkali, iron and magnesium concentrations as shown on the AFM ternary diagram of figure 5. However, two distinctive trends appear to form: a tholeiitic trend for the granites and rhyolite dykes, and a calc-alkali trend for the acid volcanics and dacite porphyry. The ternary diagram $NaAl_3SiO_8$-KAl_3SiO_8-SiO_2 of figure 6 shows similar characteristics with the granites and rhyolite dykes concentrated about the eutectic for 1 kb. isobaric equilibrium and the acid volcanics and dacite porphyry tending towards the 3 kb. isobaric equilibrium (Tuttle and Bowen, 1958). All rocks are calcium depleted which is reflected in the ternary system $Ca_2Al_2Si_2O_8$-$NaAlSi_3O_8$-$KAl_3Si_3O_8$ (figures 7a, 7b, 7c). The

Figure 5.

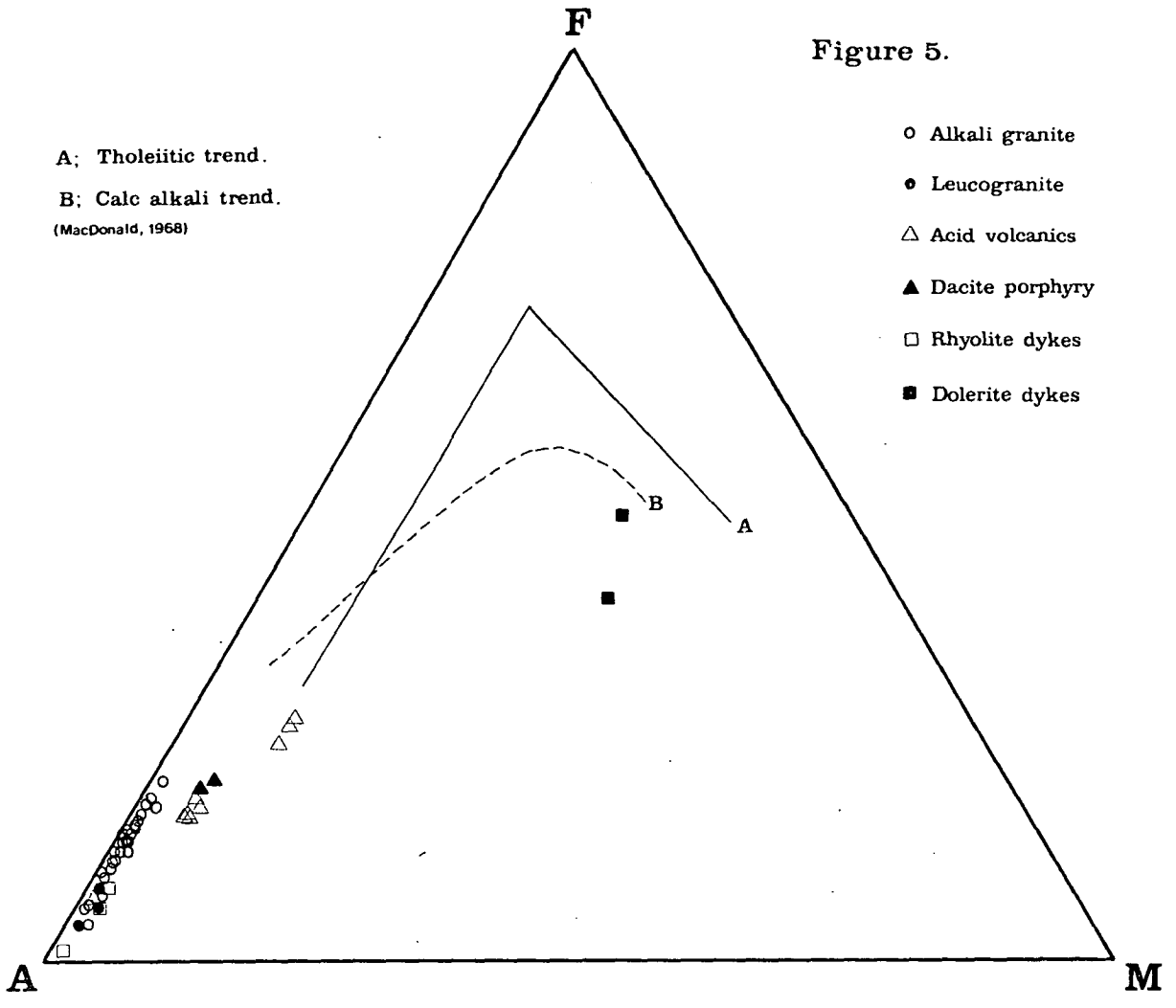

Figure 6.

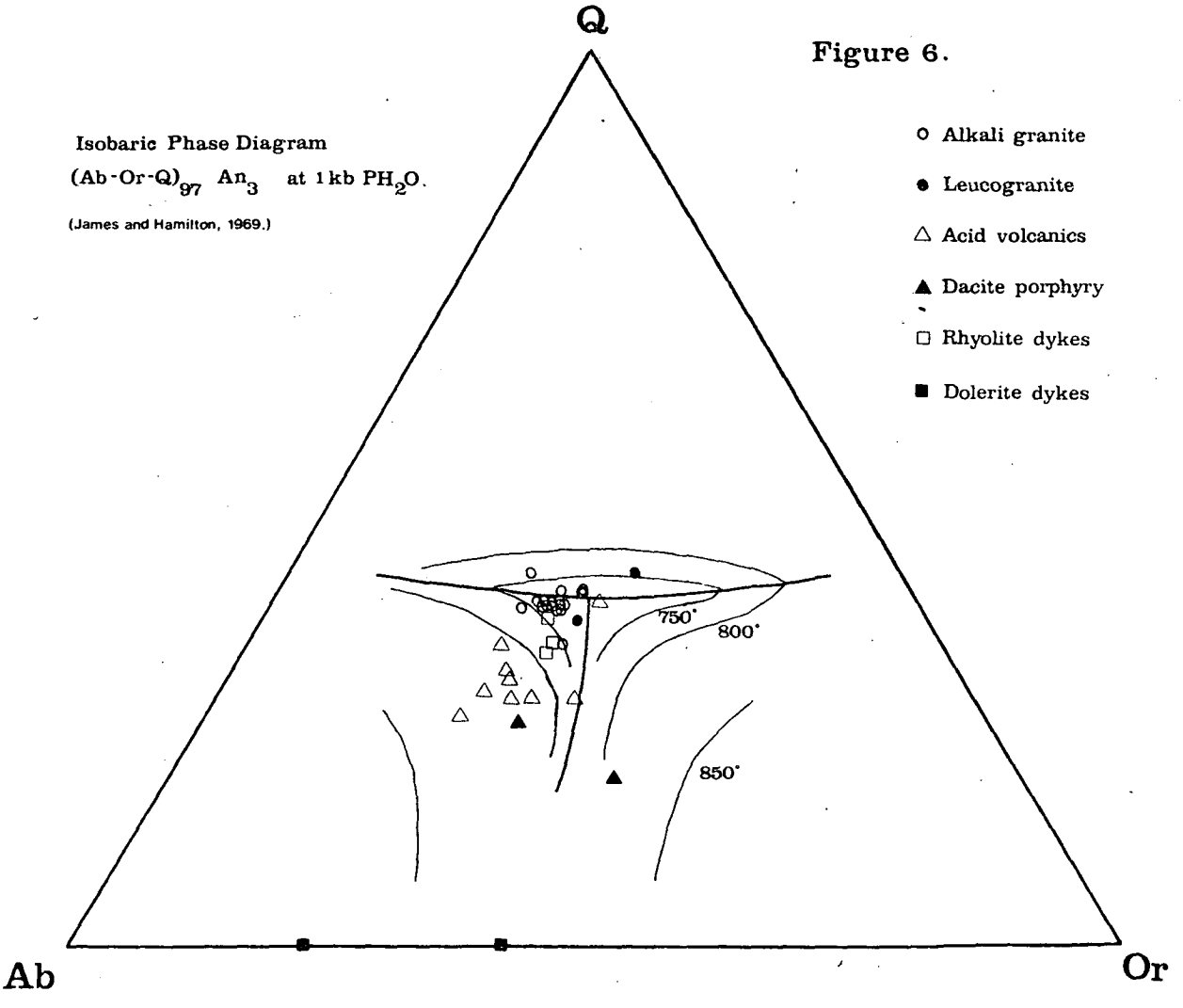

Figure 7.

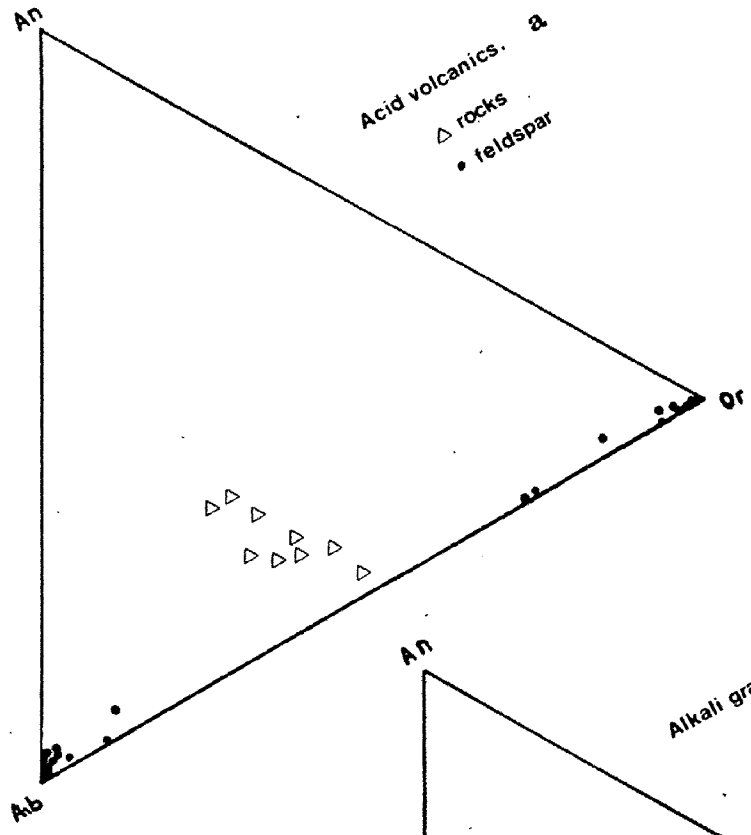
An
Ab
Or
a
Acid volcanics.
△ rocks
• feldspar

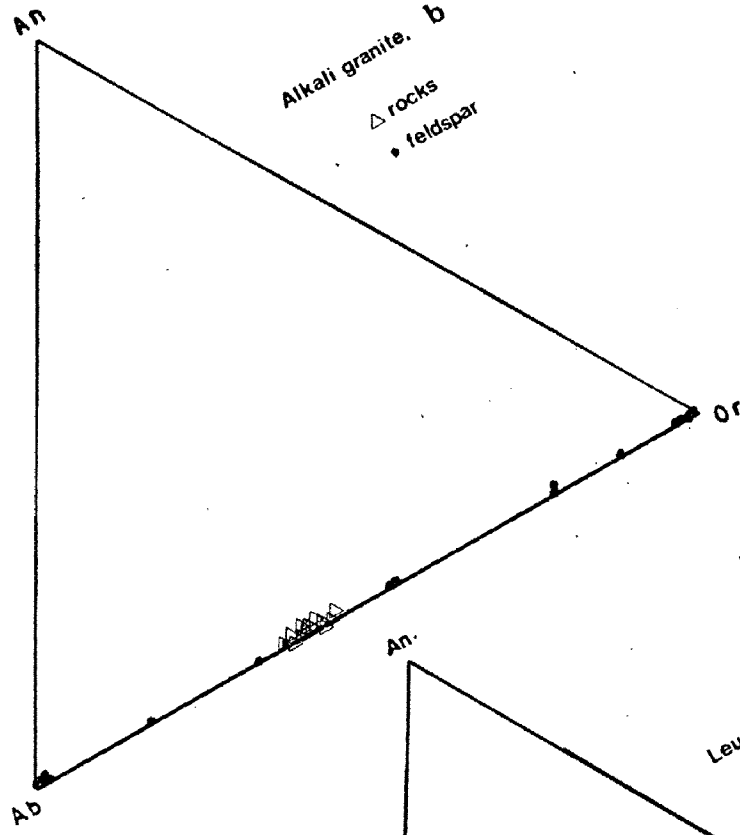
An
Ab
Or
b
Alkali granite.
△ rocks
• feldspar

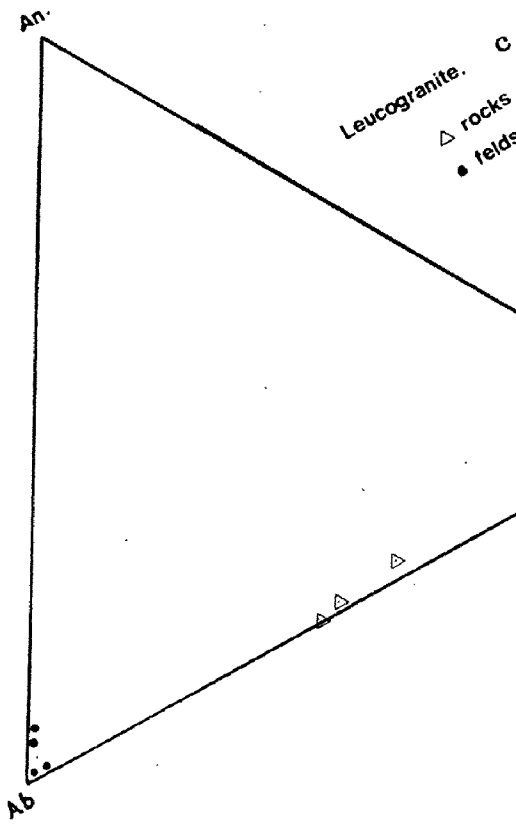
An.
Ab
c
Leucogranite.
△ rocks
• felds

acid volcanics plot along the two-feldspar equlibrium surface and the granites concentrate at the ternary minimum (Carmichael, 1976).

Adapting the C.I.P.W. normative calculations (Appendix I) to Shand's classification scheme (1927), it was found that most of the alkali granite samples and rhyolite dykes are 'peralkaline' with acmite (ac) and sodium silicate (ns) appearing in the norm. All acid volcanics can be classified as 'metaluminous' with prominent anorthite (an) in the norm and the leucogranite is 'peraluminous' with normative corundum (c). The dacite porphyry has samples both peraluminous and subaluminous.

Kuno's (1960) scheme with respect to total alkali content would classify all rocks as 'alkali' (fig. 8c) and Peacock's (1931) silica index classification system, if applicable to all lithologies, would categorise the rocks as 'alkali-calcic' (fig. 8f).

The Harker variation diagrams of SiO_2 against other major oxide components show a depletion of CaO, MgO, and P_2O_5 of the highly siliceous granites while other lithologies show a negative trend with increasing SiO_2 (fig. 8d, 9f, 9d). The iron content displays a variable range of concentrations (0.1-2.5%) in the alkali granites while the acid volcanics have a negative trend of Fe_2O_3 with respect to silica.

The total alkali content [Na_2O+K_2O] of figure 8c is consistent between all lithologies, with the exception of dolerite, ranging from 7-11%. However, K_2O has a greater range (0.7-6.3%) than Na_2O (fig. 8b).

Titanium concentration in the granites is restricted around 0.18% and is not effected by the variability of associated iron content (fig. 9a). The acid volcanics, rhyolite dykes and dacite porphyry, however, combine to produce a positive linear trend passing through the origin.

4.3 Trace element chemistry.

The zirconium content of the alkali granites have a considerable range of concentrations from 170-630 ppm (fig. 9c) while the associated silica content varies little. However, the acid volcanics and dacite porphyry show a slight negative trend with increasing silica. The rhyolite dykes have an extreme range for Zr from 110-680 ppm.

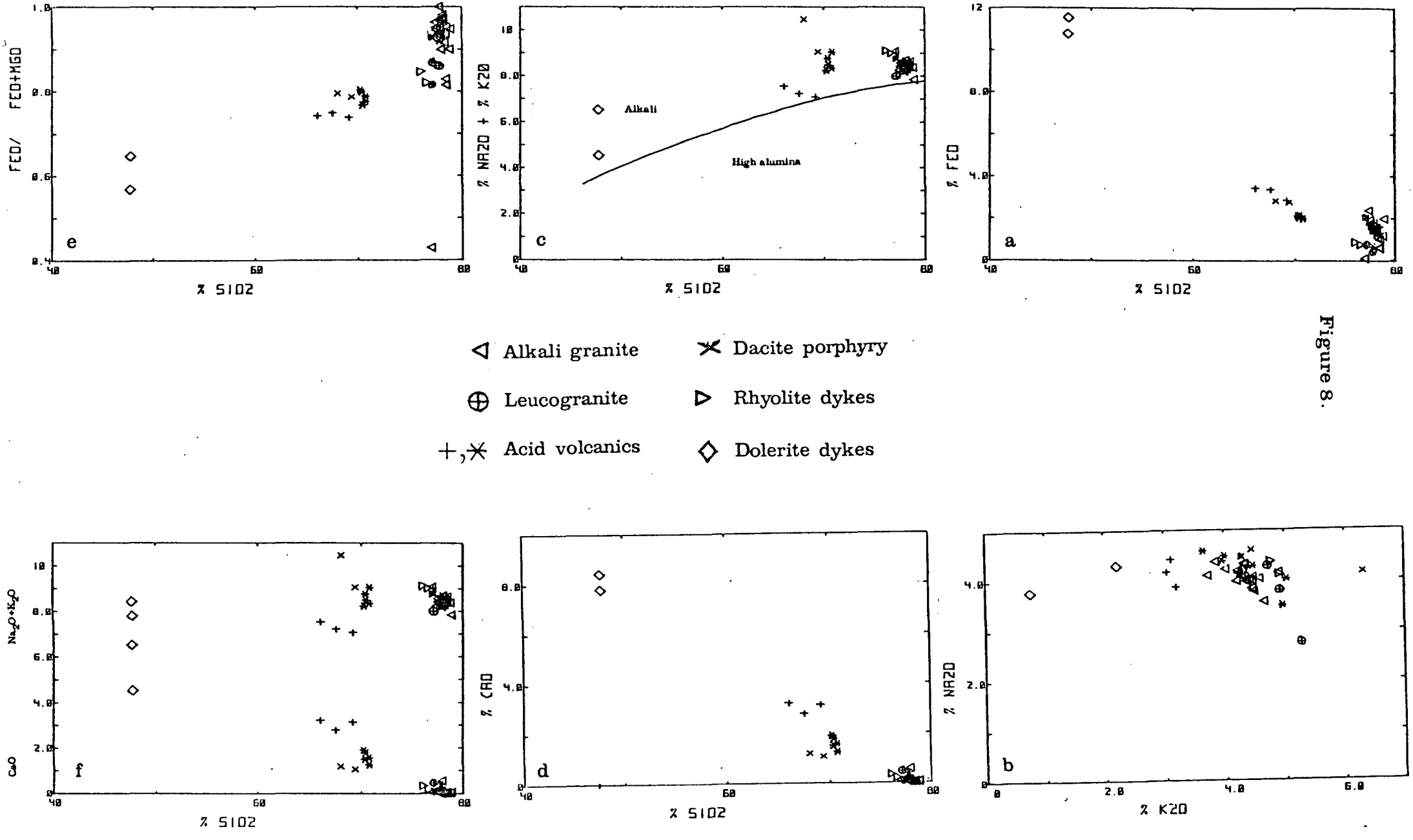
FEO/ FEO+MGO
% SIO2
e
% NA2O + % K2O
Alkali
High alumina
c
% FEO
a
Alkali granite
Leucogranite
Acid volcanics
Dacite porphyry
Rhyolite dykes
Dolerite dykes
CaO
f
% CAO
d
% NA2O
% K2O
b

Figure 8.

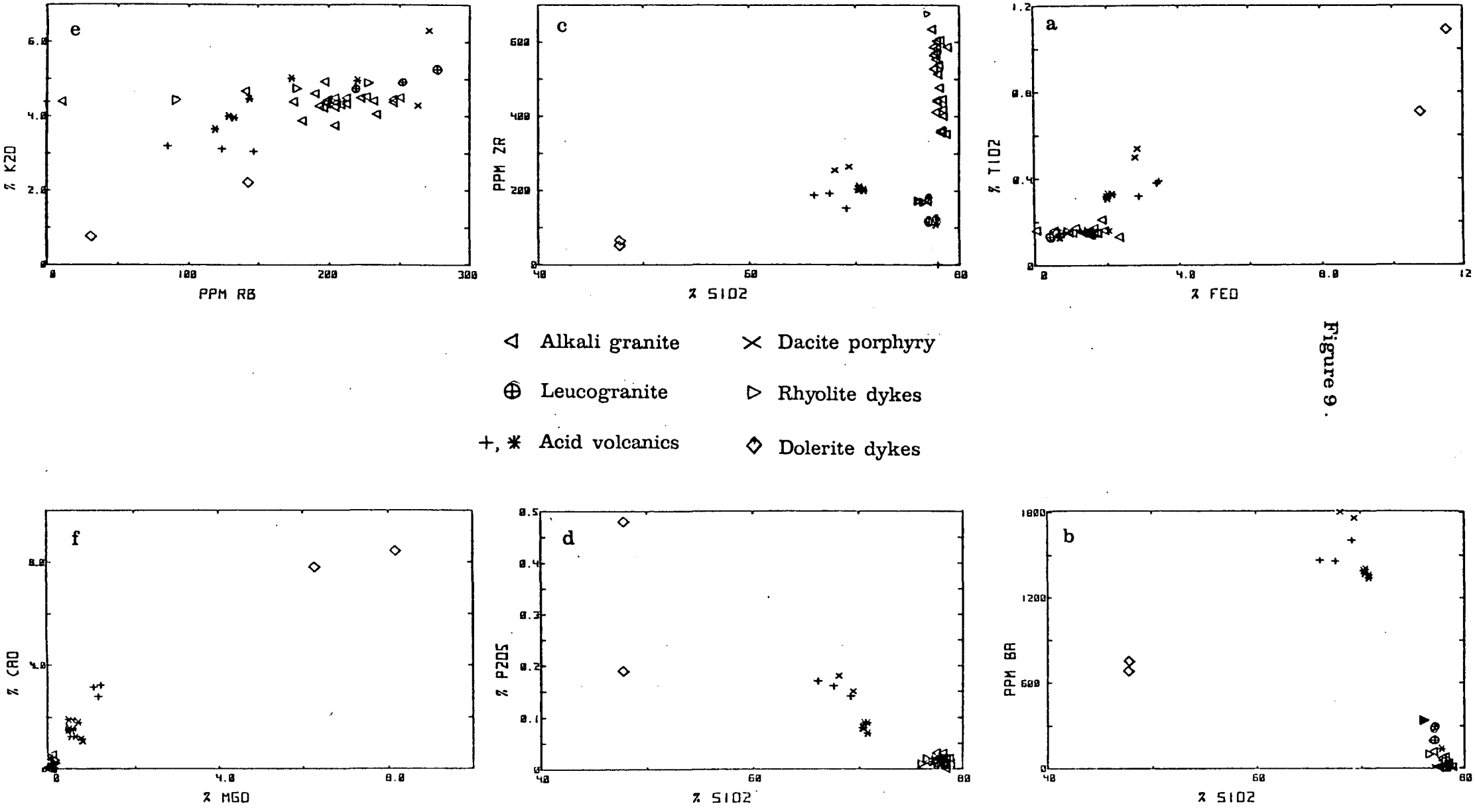
e
% K2O
PPM RB
c
PPM ZR
% SIO2
a
% TIO2
% FEO
Alkali granite
Leucogranite
+, * Acid volcanics
Dacite porphyry
Rhyolite dykes
Dolerite dykes
f
% CAO
% MGO
d
% P2O5
% SIO2
b
PPM BA
% SIO2

Figure 9.

There are two distinctive fields of barium concentrations (fig. 9b). The dacite porphyry and most of the acid volcanics show Ba enrichment (1240-1800 ppm) compared to the granites and rhyolite dykes (0-400 ppm).

Strontium has a strong positive trend passing through the origin when compared to associated calcium contents (fig. 10e). Rubidium has a positive trend for acid volcanics when compared to K_2O (fig. 9e) but has a wide range of Rb concentrations (20-200 ppm) compared to a narrow range of K_2O (3.6-4.5%). When Rb is compared to Sr (fig. 10b), the variability of Rb in Sr depleted granites becomes obvious while the acid volcanics show a negative trend.

Yttrium displays a broad range of concentrations in the alkali granite (12-78 ppm) while the acid volcanics show a much narrower range of 20-32 ppm (fig. 10a, c, d, f). This behaviour is also prevalent with niobium (fig. 10f) and zirconium (fig. 10d). However, scandium has a narrow range of 2-12 ppm for all lithologies with the exception of dolerite.

When yttrium is compared to cerium (figre 10c), three major fields can be identified: an alkali granite positive trend of approximately 0.5, an acid volcanic range of 40-120 ppm for Ce and 20-30 ppm for Y, and a high concentration of both Ce and Y in the rhyolite dykes with 50-110 ppm Y and 160 ppm Ce.

4.4 Rare earth elements.

The resultant rare earth element (REE) patterns obtained for the acid volcanic (06) and the alkali granite (38I) are shown in figre 11.

The rhyolite is enriched in light REE (Ce, Nd, Sm) relative to heavy REE (Yb) and has a negative Eu anomaly. The alkali granite is relatively depleted in all but the heaviest REE with a negative Eu anomaly. Thus the alkali granite has developed upward concaving pattern with depressed concentrations of middle REE (Sm, Eu, Gd).

If the patterns for the alkali granite and acid volcanic are typical of those that would be anticipated for other samples, then it would be possible to apply values to Ce and Nd representing the light REE, and Y representing the heavy REE from other analyses. Rare earth element patterns

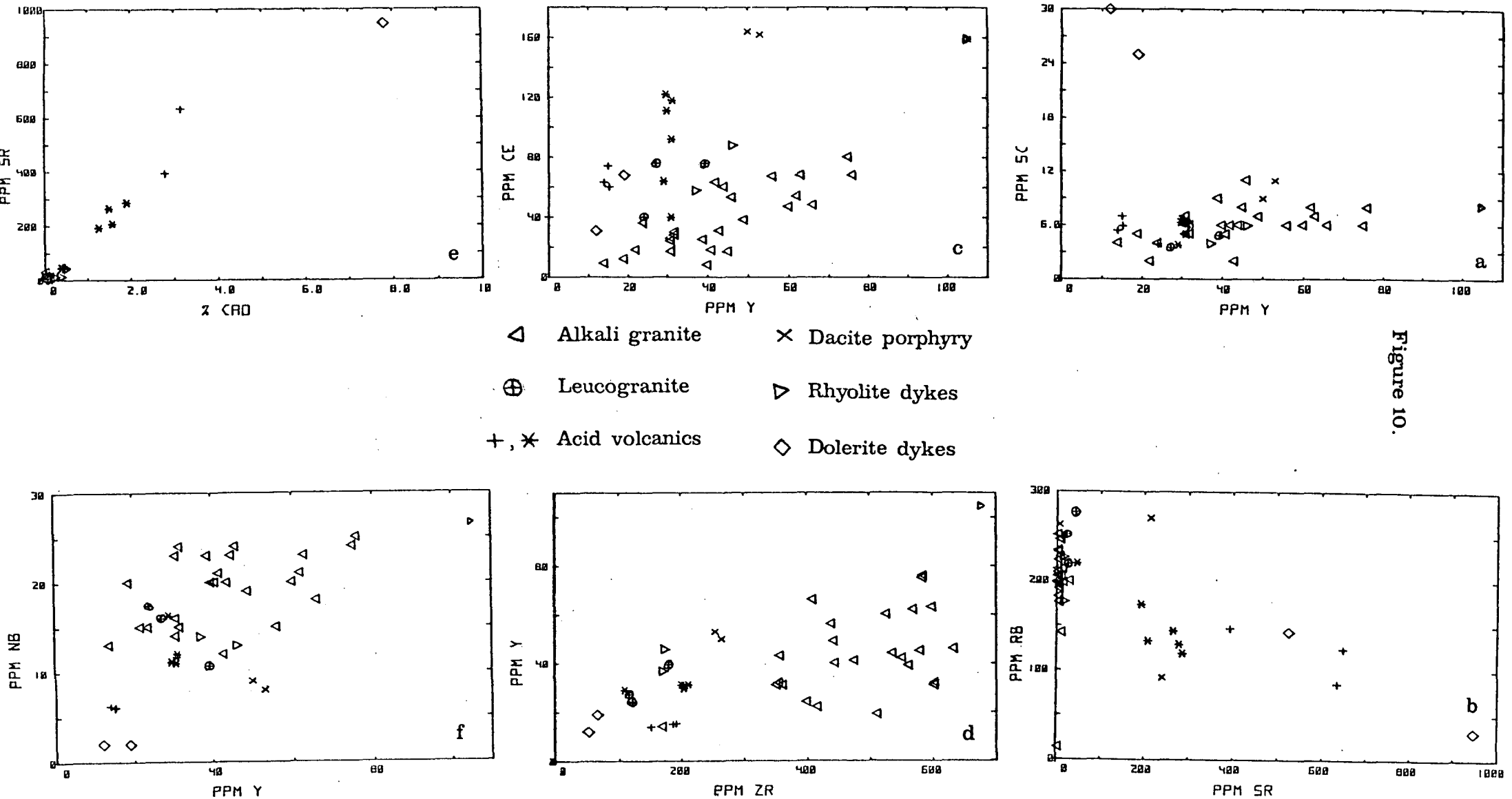
PPM SR
% CAO
e
PPM CE
PPM Y
c
PPM SC
PPM Y
a
Alkali granite
Leucogranite
Acid volcanics
Dacite porphyry
Rhyolite dykes
Dolerite dykes
PPM NB
PPM Y
f
PPM Y
PPM ZR
d
PPM RB
PPM SR
b

Figure 10.

Figure 11.

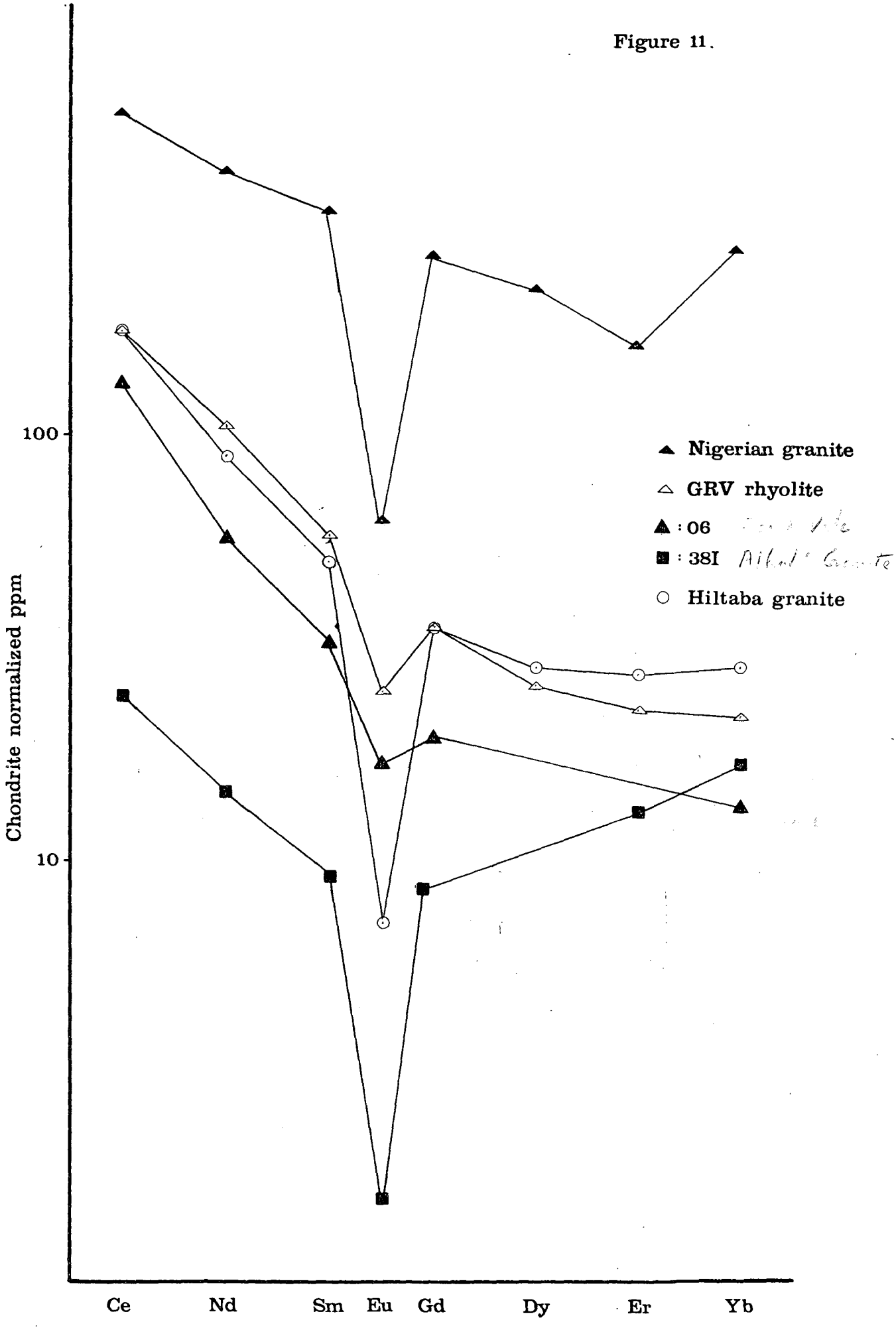
Chondrite normalized ppm
100
10
Nigerian granite
GRV rhyolite
: 06
: 38I
Hiltaba granite
Ce
Nd
Sm
Eu
Gd
Dy
Er
Yb

postulated for the acid volcanics would fluctuate up to 85 ppm for light REE, but have constant concentrations for heavy REE. However, the alkali granite REE patterns would vary in both light and heavy REE producing a series of parallel REE patterns spanding 65 ppm.

5. Mineral Chemistry.

5.1. Introduction.

Six thin sections were analysed by electron microprobe at the University of Adelaide Electron Microscopy Centre to determine chemical compositions of feldspars, oxides and mafic minerals. Two thin sections from the acid volcanics (05,06), three from the alkali granite (21,28,36) and one from the leucogranite (11) were used for the analyses.

5.2 Feldspars.

Feldspar analyses (Appendix III) are summarized in the ternary Ab-An-Or plots of figure 7, and are strongly depleted in the $CaAl_2Si_2O_8$ component (An_{07}). However, there is significant variation of the sodium content between lithologies. The acid volcanic feldspars show a restricted range of compositions between KAl_3SiO_8 (Or_{0-27}) and $NaAl_3SiO_8$ (Ab_{0-12}) in the Ab-Or solid solution series. Although the alkali granite feldspars have a concentration of compositions around the end members of the Ab-Or solid solution series, there exist intermediate compositions ranging from Ab_{0-35} for plagioclase and Or_{0-65} for alkali feldspar. The feldspar compositions for the leucogranite also concentrate around the Ab-An end members, but there may not be sufficient analyses for an accurate representation of the complete series.

The presence of abundant perthitic microcline in the alkali granite is indicative of extensive unmixing of originally homogenous alkali feldspar (Deer et al., 1966). This feature can be attributed to slower cooling at lower temperatures (Carmichael, 1976). However, the acid volcanics have strongly unmixed compositions even though the volcanics would have

crystallized quickly at higher temperatures. Low grade metamorphism and albitization may be responsible for feldspar unmixing in the acid volcanics (Bowden and Whitley, 1974).

5.3 Oxides

Microprobe analyses of opaque minerals in alkali granite samples verified the presence of ilmenite [$FeTiO_3$] and pyrophanite [$MnTiO_3$] as small lamellae within magnetite crystals. Selected analyses are given in Table 1. Pyrophanite contains a considerable amount of Fe in substitution for Mn in a ration of 5:7 (Deer et al., 1963) and ilmenite tends to be enriched in Mn when associated with magnetite (Gjelsvik, 1957).

The FeO component of magnetite and ilmenite analyses have been recalculated to ferric and ferrous iron concentrations, the procedure for which is discussed by Carmichael (1967). Thus concentrations of coexisting magnetite-ulvospinel and haematite-ilmenite solid solution series were calculated and used on the iron-titanium-oxide geothermometer of Buddington and Lindsley (1964). The maximum results obtained of the molecular percentages of ulvospinel and haematite were 22.12 and 4.45 respectively which gives a temperature of crystallization at 660^{o}C with the negative logarithm of fO_2 at 18.6 (fig. 12). Variability of the calculations noted in Table 1 are probably due to significant error from microprobe data, excessive Mn content and alteration of magnetite to haematite.

5.4 Aegirine

Aegirine, a monoclinic pyroxene, is the major mafic mineral of the alkali granite. The chemical compositions of selected aegirine microprobe analyses are given in Table 2 (21,36). This mineral commonly develops as the later product of alkaline magma crystallization (Deer et. al., op. cit.). Aegirine has been described by Jacobson et al., (1958) irregularly intergrown with reibeckite in the alkali granites of northern Nigeria. This feature has been attributed to fluctuating magma chemistry during crystallization. Alteration products of aegirine include chlorite, epidote and biotite.

Table 1.

Microprobe Analyses: Oxides

Weight percentage

		794/21			794/36	
	Il	Il	Py	Mag	Py	Py
SiO_2	0.54	0.16	0.13	0.46	2.51	2.18
TiO_2	65.64	61.58	57.51	0.05	48.47	48.23
Al_2O_3	0.37	0.08	0.11	0.03	1.23	0.03
Cr_2O_3	0.01	0.00	0.05	0.00	0.00	0.08
FeO	14.87	22.28	18.38	83.64	16.97	16.65
MnO	6.27	8.58	14.94	0.17	12.27	16.05
MgO	0.10	0.03	0.05	0.06	0.08	0.00
CaO	0.08	0.00	0.00	0.00	0.09	0.00
Na_2O	0.09	0.03	0.02	0.06	0.11	0.09
K_2O	0.02	0.00	0.01	0.00	0.05	0.00
NiO	0.00	0.02	0.01	0.02	0.00	0.09
Total	87.97	92.76	91.21	84.49	81.78	83.40
Calculated						
Fe_2O_3	-	2.24	5.67	60.85	5.27	7.12
FeO	14.87	20.19	1.322	28.81	12.75	9.99
Total	87.97	92.91	91.72	90.51	82.83	83.86
Mol % ulvospinel				0.05		
Mol % Fe_2O_3	-	1.17	3.12		3.14	4.45

Mag: magnetite, Il: ilmenite, Py: pyrophanite.

Table 1 (cont.)

	Oxides Weight percentage 794/28			
	Mag	Il	Mag	Mag
SiO_2	0.08	0.79	0.11	0.11
TiO_2	4.31	63.11	5.13	2.34
Al_2O_3	0.04	0.62	0.04	0.09
Cr_2O_3	0.02	0.01	0.05	0.03
FeO	78.90	23.71	78.92	83.34
MnO	3.20	1.20	3.09	0.64
MgO	0.00	0.19	0.01	0.06
CaO	0.00	0.04	0.00	0.00
Na_2O	0.00	0.08	0.01	0.08
K_2O	0.00	0.01	0.01	0.00
NiO	0.00	0.00	0.13	0.00
Total	86.55	89.76	87.50	86.69
Calculated				
Fe_2O_3	53.13	-	54.50	57.97
FeO	31.11	23.71	28.81	31.18
Total	91.89	89.76	91.89	92.50
Mol % ulvospinel	4.19		22.12	10.44
Mol % Fe_2O_3		-		

Mag: magnetite, Il: ilmenite, Py: pyrophanite.

Table 2.

Microprobe Analyses: Aegirine.

	Weight Percentage					
	794/21			794/36		
SiO_2	52.82	51.56	52.84	55.04	52.56	54.04
TiO_2	0.53	0.01	1.31	0.07	0.19	0.09
Al_2O_3	0.35	0.28	0.29	0.33	0.39	0.29
Cr_2O_3	0.00	0.03	0.03	0.02	0.00	0.09
FeO	29.35	29.97	29.67	30.36	30.18	30.02
MnO	0.86	0.19	0.19	0.25	0.23	0.19
MgO	0.12	0.27	0.07	0.11	0.14	0.11
CaO	0.47	0.30	0.04	0.25	0.32	0.24
Na_2O	12.96	12.83	13.33	13.58	13.12	13.52
K_2O	0.00	0.00	0.00	0.00	0.02	0.00
NiO	0.02	0.05	0.06	0.00	0.14	0.00
Total	97.48	95.49	97.83	100.01	97.29	98.59

Structural Analysis ?

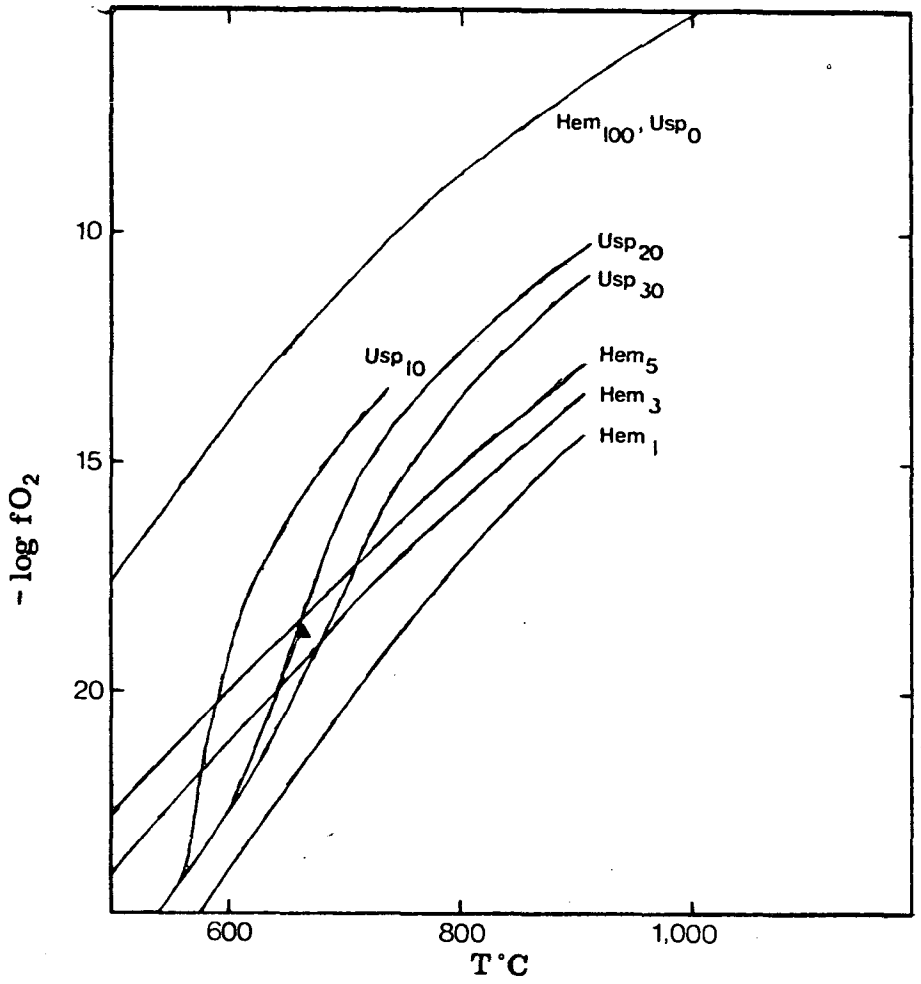

Figure 12.

Coexisting Fe–Ti oxides. Carmichael et al., 1974.

▲ Maximum obtained for alkali granite.

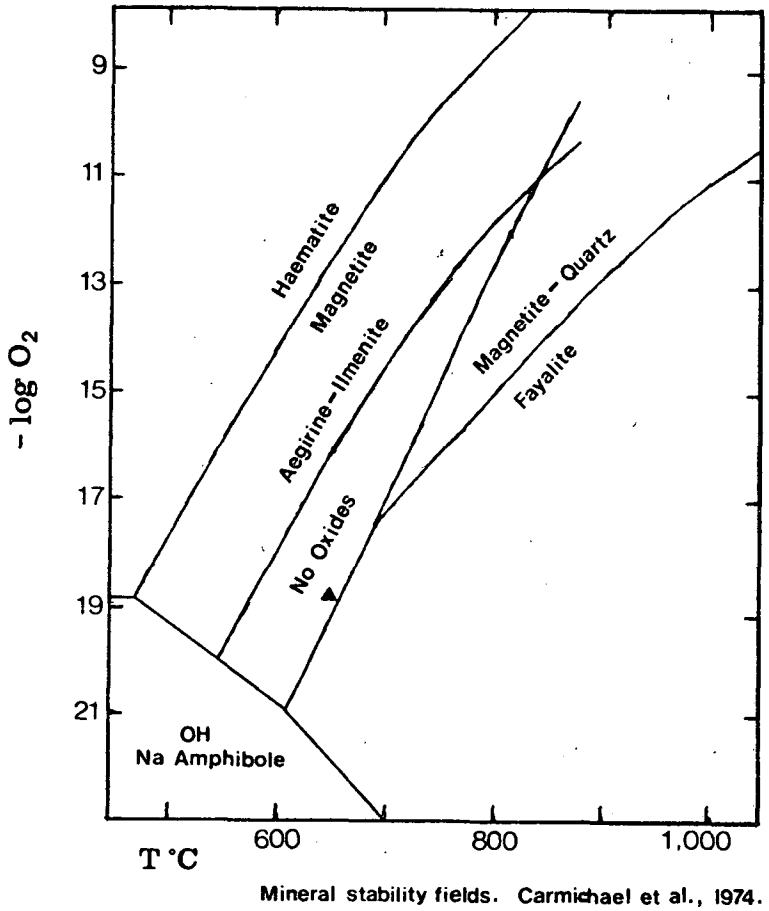

Figure 13.

Mineral stability fields. Carmichael et al., 1974.

Analyses of the aegirine closely approach the acmite end members (Sabine, 1950), have a high Na_2O and FeO content and may represent essentially hydrothermal pyroxenes developed at late magmatic and post magmatic stages (Bowden and Turner, 1973).

The presence of aegirine and oxides in the alkali granite restricts the oxygen fugacity and temperature of crystallization for which they can exist in equilibrium due to the reactions outlined by Nicholls and Carmichael (1969):

$$\underset{\text{ilmenite}}{FeTiO_3} + \underset{\text{aegirine}}{4NaFeSi_2O_6} = \underset{\text{aenigmatite}}{Na_2Fe_5TiSi_6O_{20}} + \underset{\text{liquid}}{Na_2Si_2O_5} + \underset{\text{gas}}{O_2}$$

and

$$\underset{\text{magnetite}}{4Fe_3O_4} + \underset{\text{liquid}}{6Na_2Si_2O_5} + \underset{\text{quartz}}{12SiO_2} + \underset{\text{gas}}{O_2} = \underset{\text{acmite}}{12NaFeSi_2O_6}$$

However, the calculations based on maximum molecular percentage results for oxide geothermometry in the alkali granite are outside the aegirine-magnetite-ilmenite stability field (fig. 13).

6. Comparative Geochemistry.

6.1 Introduction.

The geochemistry of the rhyolite from the acid volcanic complex and the alkali granite of Saint Francis Island is compared to geochemical results obtained from similar lithologies in the proterozoic Gawler Range volcano-plutonic complex (Giles, 1981 and Branch, 1978), the Mesozoic acid volcanics of northern Mexico (Cameron et al., 1980, 1982) and the Mesozoic granites of northern Nigeria (Bowden and Turner, 1973 and Alexiev, 1970). Major oxide and available trace element data of these complexes are recorded in Table 3 with reference to the average calc-alkali rhyolite and alkali granite compositions compiled by Nockolds (1958) and Turkekian et al. (1961).

6.2 Rhyolites.

The average rhyolite composition of Saint Francis Island (SFI) has very similar major oxide and trace element chemistry to the average calc-alkali rhyolite, with a slight enrichment in SFI rhyolite of Na_2O in exchange for CaO, twice the concentration of Sr, and 25% less iron. Like the average calc-alkali rhyolite composition, the rhyolite of the Gawler Range volcano-plutonic complex is depleted in Na_2O and Sr, enriched in K_2O and Rb, and is strongly depleted in CaO.

The Mesozoic acid volcanics of Chihuahua, northern Mexico are very similar to the SFI rhyolite in both major oxide and trace element concentrations. They have been described by Cameron et al. (1980) as peraluminous with normative corundum less than 1.6% and calc-alkali due to minor iron enrichment. MgO accounted for less than 0.25% of the Chihuahua rhyolite with 4% K_2O at 75% SiO_2, and Na_2O averaging 4%. Trace element concentrations showed Sr increased with SiO_2 and the presence of hornblende or pyroxene was responsible for lower and higher contents respectively.

Rare earth element (REE) studies on rhyolites of northern Mexico (Cameron et al., 1982) show that the pattern and field of variation of the Chihuahua rhyolites is very similar and encompasses that of the SFI rhyolite (06). However, SFI rhyolites may have a broader field of variation for light REE if postulated trends for all rhyolite samples are included.

The calculated REE pattern for Chihuahua rhyolite by fractional crystallization of an andesite parent closely resembles that of SFI rhyolite 06. This calculation was based on 25% removal of plagioclase, pyroxene and Fe-Ti oxides from an andesite followed by 35% removal of hornblende, plagioclase and Fe-Ti oxides from the resultant dacite.

Comparison of the REE pattern of a rhyolite (71% SiO_2) from the Lake Everard area of the Gawler Range volcano-plutonic complex (Giles, 1981) shows a similar trend but is more enriched in all REE with a more prominent negative Eu anomaly and a relatively higher concentration of heavy REE (fig. 11).

Table 3.

Average Rhyolite Compositions.

	SFI	AVR	GRV	NMR
SiO_2	72.85	73.66	75.52	74.52
TiO_2	0.27	0.22	0.27	0.34
Al_2O_3	13.87	13.45	12.33	13.58
Fe_2O_3	0.75	1.25	1.90	1.77
FeO	0.75	0.75	0.28	0.14
HnO	0.08	0.03	0.03	0.08
MgO	0.39	0.32	0.22	0.46
CaO	1.18	1.13	0.26	1.36
Na_2O	3.92	2.99	2.96	4.16
K_2O	4.55	5.35	5.15	3.55
P_2O_5	0.06	0.07	0.06	0.06
Rb	132	170	202	159
Sc	214	100	72	195
Ba	1168	846	1597	NA
Zr	189	175	296	263
Nb	12	21	20	16
Y	30	40	43	38

NA: Not available
SFI: Saint Francis Island acid volcanic rhyolite.
AVR: Average calc-alkali rhyolite.
GRV: Gawler Range volcano-plutonic complex rhyolite.
NMR: Rhyolite from Chihuhua, Mexico.

Thus the Saint Francis Island rhyolite is very similar to other calc-alkali rhyolites but can be distinguished by a very low iron and an unusually high strontium concentrations.

6.3 Granites.

The alkali granite of Saint Francis Island shows some remarkable variations from the average alkali granite of Nockolds (1958). Although the alkali and aluminia contents are similar, the SFI alkali granite has 7% more silica and is thus relatively depleted in all other major oxides. Trace element comparison also shows significant variation from the average (Turekian et al. 1961). Sr and Ba are extremely depleted while Zr has more than twice the average concentrations in the SFI alkali granite.

The proterozoic Hiltaba Granite of the Gawler Range volcano-plutonic complex (Giles, 1981 and Branch, 1978) has nearly identical major oxide concentrations with the exception of slightly more enriched K_2O and CaO in exchange for Na_2O in comparison with the SFI alkali granite. Like the average alkali granite trace element concentrations, the Hiltaba Granite is relatively enriched in Sr, Ba and depleted in Zr compared to the SFI alkali granite.

The chemical characteristics of the peralkaline Mesozoic granites of northern Nigeria include a deficientcy of Al relative to K, low Ca and Mg (Bowden and Turner, 1976). The SFI alkali granite differs from the Nigerian granites by having a greater deficiency in all major oxides, especially iron, and an enrichment in silica. Zr, Y and Nb are enriched and Rb is depleted in the Nigerian granites compared to the SFI alkali granite. However, Sr and Ba are markedly depleted in both the SFI granite and the Nigerian alkali granites. Thus major oxide and trace element characteristics for the SFI alkali granite include enriched SiO_2 and Zr, and depleted total iron, CaO, Sr and Ba.

The rare earth element pattern of the SFI alkali granite (38I) is depleted in all elements relative to that from the Hiltaba Granite (76.6% SiO_2) (Giles, 1981), and has a positive trend for increasing heavy REE concentrations compared to the constant concentrations for the Hiltaba Granite

Table 3 (cont.)

Average Granite Compositions.

	SFI	AVR	HG	GG
SiO_2	78.06	71.08	76.42	74.05
TiO_2	0.16	0.40	0.16	0.35
Al_2O_3	11.19	11.26	11.89	11.20
Fe_2O_3	0.75	4.28	0.90	2.10
FeO	0.75	2.19	0.70	1.70
HnO	0.07	0.11	0.03	0.10
MgO	0.08	0.25	0.10	0.40
CaO	0.06	0.84	0.39	0.45
Na_2O	4.13	4.92	2.97	4.60
K_2O	4.36	4.21	5.29	5.20
P_2O_5	0.02	0.07	0.04	0.06
Rb	219	170	320	160
Sc	5	100	38	NA
Ba	6	846	357	NA
Zr	492	175	239	1250
Nb	20	21	22	100
Y	47	40	44	120

NA: Not available
SFI: Saint Francis Island alkali granite.
AVR: Average peralkaline granite.
HG: Hiltaba Granite, Gawler Range volcano-plutonic province.
GG: Aegirine granite of Goure, northern Nigeria.

(fig. 11). Compared to the average REE pattern from nine peralkaline granites from northern Nigeria (Alexiev, 1970) (fig. 11), both the Hiltaba and SFI 38I granites are relatively depleted in all REE. Thus the characteristic pattern of the SFI alkali granite 38I is not only a depleted total REE count, but also an enriched heavy REE relative to light REE.

7. Petrogenesis.

The presence of feldspar phenocrysts and partially resorbed quartz phenocrysts in the extrusive rhyolite of the acid volcanic complex are indicative of initial slow cooling crystallization in equilibrium with the liquid phase at depth which later became in inequilibrium at surface conditions and began to be assimilated into the melt prior to complete crystallization of the lava pile (Cox et al., 1979). Like the rhyolite, the dacite intrusives of the acid volcanic complex display this feature. Collectively, the rhyolite and dacite form convincing trends of decreasing total Fe_2O_3, MgO, CaO, P_2O_5 and TiO_2 with increasing silica content. They also plot in similar temperature - pressure fields of the $NaAlSi_3O_8$-$KAlSi_3O_8$-SiO_2 and $NaAl_3SiO_8$-KAl_3SiO_8-$CaAl_2Si_2O_6$ systems. Such cohesive chemical and petrographic behavior suggests formation by means of progressive crystal fractionation of a more mafic source magma.

Rhyolite is too siliceous to have evolved from ultramafic material (Stern, 1973). However, it is most likely to represent the low melting fraction of crustal rocks at crustal pressures (Wyllie, 1977). Partial melting of crustal material at lower crustal regions can develop voluminous rhyolitic melts (Eichelberger, 1978). As the lower crust is likely to be the hotest source region and of gabbroic or intermediate composition (Green and Ringwood, 1968) rather than granitic, rhyolite would have to evolve from collectively small volumes of partial melting. In order to generate a heat source for lower crustal melting, Younker and Vogen (1976) have suggested that this could be accomplished by heat transfer from mantle basaltic magmatism. However, the lack of andesitic zonation of plagioclase feldspar phenocrysts (An_{45-65}) in the rhyolite accompanied by the lack of comagmatic mafic volcanism argues against mafic hybridization.

The compatible elements Ni and Sc are strongly depleted in the acid volcanics as a result of early removal of olivine and pyroxene from the melt by means of fractional crystallization (Taylor, 1966). The characteristic high Ba content can also be accounted for by fractional crystallization as it behaves like an incompatible element concentrating in the residual phases until the crystallization of biotite and alkali feldspar (Schnetzler and Philpotts, 1968). The narrow range of concentrations of the highly incompatible elements Nb, Y and Zr reflect the consistency of the residual phases during the fractional crystallization process. Zr shows a slightly decreasing trend with increasing silica suggesting the precipitation of crystallizing zircon during the later phase of fractionation (Nagasawa, 1970).

The REE pattern of rhyolite of the acid volcanic complex conforms to other similar examples derived by fractional crystallization. Most noted is the similarity of the pattern contrived by Cameron et al. (1982) by means of 77-83 wt. % phenocryst fractionation from an andesite parent.

In contrast, the alkali granite has many features which are more characteristic of genesis by means of partial melting of sialic crustal material. The granite has prominent graphic texture of intergrown quartz and alkali feldspar along with a noted abundance of perthitic feldspar and Q-Ab-An-Or systems plots all of which are indicative of low temperature, low pressure eutectic melt conditions. The granite also has all the criteria of White et al. (1977) for minimum melt genesis including about 76% SiO_2, absence of zoned plagioclase and depleted Mg and Ni. Geothermometry based on coexisting magnetite-ilmenite exsolution lamellae indicates low temperature conditions of oxide crystallization (660%C). Experimental studies by Bailey (1969) on melts of acmite composition has shown that the reduction of PO_2 can lower the melting range by over 170^{o} and yield an alkali rich liquid for the generation of low temperature peralkaline melts. However, the temperature and PO_2 conditions suggested for genesis of the alkali granite are not within the acmite - ilmentite - Fe - Ti oxide - magnetite stability field of Nicholls and Carmichael (1969).

The broad range of concentrations in the alkali granite of the highly incompatible elements Nb, Y and Zr cannot be accounted for by the fractional crystallization process (Gast, 1968). Thus the alkali granite melt must have

been randomly contaminated during partial melting by variable quantities of source rock minerals such as zircon which harbour these elements.

The rare earth element pattern obtained for the alkali granite quite clearly cannot be formulated by fractional crystallization to account of the strong depletion in all but the heaviest REE as fractional crystallization tends to concentrate REE in the residual phases (Nagasawa and Schnetzler, 1970). However, low fractions of partial melting would prevent large increases in REE relative to the parent (Shaw, 1970). Progressive albitization of perthitic feldspar and lack of amphibole incorporated into the alkali granite melt from source material may be responsible for the depleted middle REE concentrations (Bowden and Whitley, 1972 and Arth and Barker, 1976). The large negative Eu anomaly is due to the lack of plagioclase assimilation into the melt, and the relatively enriched heavy REE concentration is related to the presence of zenocrystic zircon (Nagasawa, 1970).

Granite types reflect tectonic environment. Although most granites are calc-alkaline due to shallow melting on continental margins, alkaline granites are important in Proterozoic intraplate crustal development (Emslie, 1978). Bridgewater et al. (1974) suggest that alkaline magmatic activity during mid-Proterozoic time (1500-2000 ma) may reflect inefficient coupling between lithosphere and asthenosphere.

Like the alkali granite, the leucogranite of the acid volcanic complex and the rhyolite dykes of the alkali granite complex display many petrographic and geochemical features indicative of low pressure-temperature eutectic melt conditions such as perthitic feldspars, graphic intergrowths low CaO, MnO, MgO, total Fe_2O_3, TiO_2, P_2O_5 and high SiO_2. However, the leucogranite and rhyolite dykes do not contain aegirine and have higher Ba concentrations. The rhyolite dykes lack Fe-Ti oxides and show little alteration. Thus although most petrographic and geochemical evidence indicates that the leucogranite and rhyolite dykes developed in a similar environment to that of the alkali granite, mineralogical differences suggest evolution from more iron depleted melts. The lack of significant alteration in the rhyolite dykes indicate that the intrusion was post alteration which had effected all other lithologies except dolerite to varying degrees.

The chemistry of the magacrystic dacite porphyry behaves cohesively to those characteristics of the acid volcanics such as related pressure-temperature melt conditions following decreasing trends of total Fe_2O_3, MgO, CaO, TiO_2 and P_2O_5 with respect to increasing silica. The lack of zonation within the alkali feldspar megacrysts suggests that the intratelluric porphyry dacite may represent primitive unfractionated melt conditions and the lack of any significant contact margin may indicate that the intrusion occurred into an already hot granite host.

In order to develop the non minimum melt characteristics, the porphyry dacite must have formed from lower crustal regions and may represent a renewed phase of lower crustal melting followed by extrusion along arcuate fractures into shallow crustal levels. The renewed supply of mantle heat that created the megacrystic dacite melt at lower crustal levels may have subsequently caused shallow crustal minimum eutectic melting that resulted in the creation of the rhyolite dykes which intrude the alkali granite.

The initial $^{87}Sr/^{86}Sr$ for the alkali granite has been calculated by Webb et al. (1981) as 0.7114 $\pm$ 0.0032 to give an age of 1478 $\pm$ 15 ma. Using the mean age of 1500 ma, Hurley (1968) has calculated the average initial $^{87}Sr/^{86}Sr$ for major divisions of the earth:

Upper continental crust: initial $^{87}Sr/^{86}Sr$ = 0.7205
Lower continental crust: initial $^{87}Sr/^{86}Sr$ = 0.7045
Oceanic basalt : initial $^{87}Sr/^{86}Sr$ = 0.7035

In comparison, the alkali granite has a relatively high Sr ratio which would be indicative of upper continental crustal genesis. Small amounts of partial melting of average crustal rocks will also produce liquids enriched in Rb and have a high Sr ratio (Powell and Bell, 1974). The probable source rock for the alkali granite is late Archaean gneiss which crops out in southern Eyre Peninsula, South Australia (Cooper et al., 1976). Initial $^{87}Sr/^{86}Sr$ and average Rb concentration of the Cape Carnot leucogneiss, the oldest lithology recorded (2838 $\pm$ 563 ma), is 0.7026 $\pm$ 102 and 60 ppm respectively. Thus it is feasable that shallow partial melting of the leucogneiss can significantly raise the $^{87}Sr/^{86}Sr$ and Rb ppm to levels similar to those obtained from the alkali granite.

In contrast, the initial Sr ratio for the acid volcanics (0.7056 ± 0.0005) which gives an age of 1490 ± 12 ma, is more conducive to genesis at lower crustal conditions. The $^{87}Sr/^{86}Sr$ value of the leucogranite (0.7088 ± 0.00034), which gives an age of 1489 ± 15 ma, is intermediate of both the alkali granite and acid volcanics, perhaps indicating lower crustal melt contamination during shallow crustal formation.

The intrusion of subvertical dolerite dykes represent the final magmatic stage in the crystalline basement of Saint Francis Island. Contemporanous dolerite dyke swarms have been recognised to occur on several continents and reflect widespread stable tectonic conditions or indicate early rifting along continental margins (Windley, 1977).

8. Conclusions.

The crystalline basement of southwest Saint Francis Island corresponds to the mid Proterozoic Gawler Range volcano-plutonic complex. Mantle magmatism may have been responsible for initial lower crustal melting followed by fractional crystallization to produce the sequence of tuffaceous acid volcanics. The influx of high temperature magma into shallow crustal levels induced partial eutectic melting for the subsequent development of the alkali granite pluton which intruded into the volcanic pile. Renewed lower crustal magmatism resulted in the intrusion of the megacrystic dacite porphyry dyke which in turn encouraged partial shallow crustal melting and resulted in the formation of the rhyolite dykes. The intrusion of the dolerite dykes represent the final magmatic event on Saint Francis Island.

The alkali granite, characterized by the presence of aegirine, represents a chemically different pluton to those described intruding the acid volcanics of the Gawler Range volcano-plutonic complex. The leucogranite, although genetically similar to that of the alkali granite, is also chemically different indicating variations in magma composition.

Acknowledgements.

The author wishes to express sincere gratitude for the assistance received from members of the Department of Geology and Mineralogy of the University of Adelaide.

With respect to geochemical analyses, P. McDuie aided in whole rock preparation, J. Stanley accomplished major oxide and trace element spectrometry, K. Turnbull assisted in REE preparations and J. Foden executed REE spectrometry.

Microprobe work was completed under the supervision of Dr. Brendon Griffin at the University of Adelaide Electron Optical Centre.

Fieldwork was undertaken under the sapient guidance of Dr. John Cooper and manuscript typing was completed by Ms. Sandra Storer.

The supervisor of this thesis, Dr. John Foden, deserves the heartiest of thanks for his enthusiastic encouragement and sagacious councel in all aspects of thesis development.

References cited.

Alexiev, E.I., 1970. Rare earth elements in younger granites of northern Nigeria and the Cameroons and their genetic significance. Geokhimiya 2, 192-198.

Arth, J.G. and F. Barker, 1976. Rare earth partitioning between hornblende and dacitic liquid and implications for the genesis of trondhjemitic - tonalitic magmas. Geology 4, 534-536.

Bailey, D.K., 1969. The stability of acmite in the presence of H_2O. Am. J. Sci. 267-A, 1-16.

Bowden, P. and J.E. Whitley, 1974. Rare earth patterns in peralkaline and associated granites. Lithos 7, 15-21.

Bowden, P. and D.C. Turner, 1973. Peralkaline and associated ring-complexes in the Nigeria - Niger province, West Africa. The Alkaline Rocks, Sorensen, H. John Wiley, New York.

Branch, C.D., 1978. Evolution of the middle proterozoic Chandabooka caldera, Gawler Range acid volcano-plutonic province, South Australia. J. Geol. Soc. Aust. 25, 199-216.

Bridgewater, D., J. Sutton and J. Watterson, 1974. Crustal downfolding associated with igneous activity. Tectonophysics 21, 57-77.

Buddington, A.F. and D.H. Lindsley, 1964. Iron-titanium oxide minerals and synthetic equivalents. J. Petrol. 5, 310-357.

Cameron, M., W.C. Bagby and K.L. Cameron, 1980. Petrogenesis of voluminous mid-Tertiary ignimbrites of Sierra Hadre Occidental, Chihuahua, Mexico. Contrib. Mineral. Petrol. 74, 271-284.

Cameron, L.C. and N.H. Gilbert, 1982. Rare earth element evidence concerning the origin of voluminous mid-Tertiary rhyolitic ignimbrites and related volcanic rocks, Sierra Madre Occidental, Chihuahua, Mexico. Geochim. Cosmochim. Acta 46, 1486-1503.

Carmichael, I.S.E., 1967. Iron-titanium oxides of sialic volcanic rocks and their associated ferromagnesian silicates. Contrib. Mineral. Petrol. 14, 36-64.

Carmichael, I.S.E., F.J. Turner and J. Verhoogen, 1974. Igneous petrology. McGraw-Hill, New York.

Carmichael, I.S.E., 1976. The crystallization of feldspar in volcanic acid liquid. J. Geophys. Res. 72, 4665-4687.

Cooper, J.A., C.M. Fanning, M.M. Flook and R.L. Oliver, 1976. Archaean and proterozoic metamorphic rocks on southern Eyre Peninsula, South Australia. J. Geol. Soc. Aust. 23, 287-292.

Cox, K.G., J.D. Bell and R.J. Pankhurst, 1979. The interpretation of igneous rocks. George Allen and Unwin, London.

Deer. W.A., R.A. Howie and J. Zussman, 1962. Rock forming minerals. Longmans, Green and Co. Ltd., London.

Deer, W.A., R.A. Howie and J. Zussman, 1966. An introduction to rock forming minerals. Longmans, Green and Co. Ltd., London.

Eichelberger, J.C., 1978. Andesitic volcanism and crustal evolution. Nature 275, 21-27.

Emslie, R.F., 1978. Anorthosite massifs, rapakivi granites and late proterozoic rifting of North America. Precambrian Res. 7, 61-98.

Flint, R.B. and A.F. Crooks, 1981. Geology of St. Francis and West Islands, Nuyts Archipelago. S. Aust. Dept. Mines and Energy report 82/10 (unpublished).

Gast, P.W., 1968. Trace element fractionation and origin of tholeiitic and alkaline magma types. Geochim. Cosmochim. Acta 32, 1057-1086.

Giles, C.W., 1980. A comparative study of Archaean and Proterozoic felsic volcanic associations in Southern Australia. University of Adelaide unpublished Ph.D. thesis.

Gjelsvik, T., 1957. Geochemical and mineralogical investigation of titaniferous iron ores, west coast of Norway. Econ. Geol. 52, 482-498.

Green, T.H. and A.E. Ringwood, 1968. Genesis of the calc-alkaline igenous rocks suite. Contrib. Mineral. Petrol. 18, 105-162.

Hurley, P.M., 1968. Absolute abundances and distributions of Rb, K and Sr in the earth. Geochim. Cosmochim. Acta 32, 273-283.

Jacobson, R.R.E., W.N. MacLeod, and R. Black, 1958. Ring-complexes in the younger granite province of northern Nigeria. Geol. Soc., Mem. No. 1.

James, R.S. and D.L. Hamilton, 1969. Phase relations in the system $NaAlSi_3O_8$ - $KAlSi_3O_8$ - $CaAl_2Si_2O_8$ - SiO_2 at one kilobar water vapour pressure. Contrib. Mineral. Petrol. 21, 111-141.

Kinsman, J.E., 1973. Photogeological interpretation of the islands of the western Continental Shelf, South Australia. S. Aust. Dept. Mines and Energy report 73/125 (unpublished).

Kuno, H., 1960. High-alumina basalt. J. Petrol. 1, 121-45.

MacDonald, G.A. and T. Katsura, 1964. Chemical composition of Hawaiian lavas. J. Petrol. 5, 82-133.

Major, R.B., 1973. Preliminary report: geology of the islands of the western Continental Shelf of South Australia. S. Aust. Dept. Mines and Energy report 73/226 (unpublished).

Nagasawa, H., 1970. Rare earth concentrations in zircons and apatites in their host dacites and granites. Earth Planet. Sci. Lett. 9, 359-346.

Nagasawa, H. and C.C. Schnetzler, 1971. Partitioning of rare earth, alkali and acid igenous magma. Geochim. Cosmochim. Acta 35, 953-968.

Nicholls, J. and I.S.E. Carmichaeal, 1967. Iron-titanium oxides and ocygen fugacities in volcanic rocks. J. Geophys. Res. 72, 4665-4687.

Nockolds, S.R., 1954. Average chemical compositions of some igneous rocks. Bull. Geol. Soc. Am. 65, 1007-1032.

O'Connor, J.T., 1965. A classification of quartz-rich igenous rocks based on feldspar rations. U.S. Geol. Surv. Prof. Pap. 252B, 79-84.

Peacock, M.A., 1931. Classification of igneous rock series. J. Geol. 39, 54-67.

Powell, J.L. and K. Bell, 1974. Isotopic composition of strontium in alkalic rocks. The Alkaline Rocks, H. Sorensen ed. John Wiley, New York.

Price, N.S., 1966. Fault and joint development in brittle and semi-brittle rock. Permagon Press Ltd., London.

Sabine, P., 1950. Optical properties and compositions of acmite pyroxenes. Mineralog Mag. 29, 113-115.

Schnetzler, C.C. and J.A. Philpotts, 1968. Partition coefficients of rare earth elements and barium between igenous matrix materials and rock forming mineral phenocrysts - II. Geochim. Cosmochim. Acta 34, 331-340.

Shand, S.J., 1927. The eruptive rocks. Wiley, New York.

Shaw, D.M. 1970. Trace element fractionation during anatexis. Geochim. Cosmochim Acta 34, 237-243.

Stern, C.R. and P.J. Wyllie, 1973. Crustal compositions at mantle pressures. Earth Planet Sci. Lett. 18, 163-167.

Taylor, S.R., 1966. The application of trace element data to problems in petrology. Physics and Chemistry of the Earth 6, 133-213.

Turekian, K.K. and K.H. Wedopohl, 1961. Distribution of the elements in some of the major units of the earth's crust. Geol. Soc. Amer. Bull. 72, 175-192.

Turner, A.R., 1975. Petrology of the eastern Gawler Ranges volcanic complex. Bull. geol. Surv. S. Aust., 45.

Tuttle, O.F. and N.L. Bowen, 1958. Origin of granite in the light of experimental studies in the system $NaAl_3Si_3O_8$ - $KAlSi_3O_8$ - SiO_2 - H_2O. Geol. Soc. Am. Mem. 74.

Walker, N.C. and S.J. Botham, 1969. Reconnaissance geological survey of the Streakey Bay and Nuyts 1: 250 000 areas. S. Aust. Dept. Mines and Energy report 68/25 (unpublished).

Webb, A.W., 1979. A geochronological investigation into the tectono-magmatic history of the Gawler Craton. Symposium on the Gawler Craton, extended abstracts, Geol. Soc. Aust., Adelaide. Compiled by A.J. Parker.

White, A.J.R. and B.W. Chappell, 1977. Ultrametamorphism and granitoid genesis. Tectonophysics 43, 7-22.

Windley, B.F., 1977. The evolving continents. John Wiley and Sons Ltd. Chichester, U.K.

Wyllie, P.J., 1977. Crustal anatexis: an experimental review. Tectonophysics 43, 41-71.

Younker, L.W. and T.A. Vogel, 1976. Plutonism and plate dynamics: the origin of circum - Pacific batholiths. Can. Mineral. 14, 238-244.

Sample location map 3.

Scale 1 : 15,746.

0 m 500

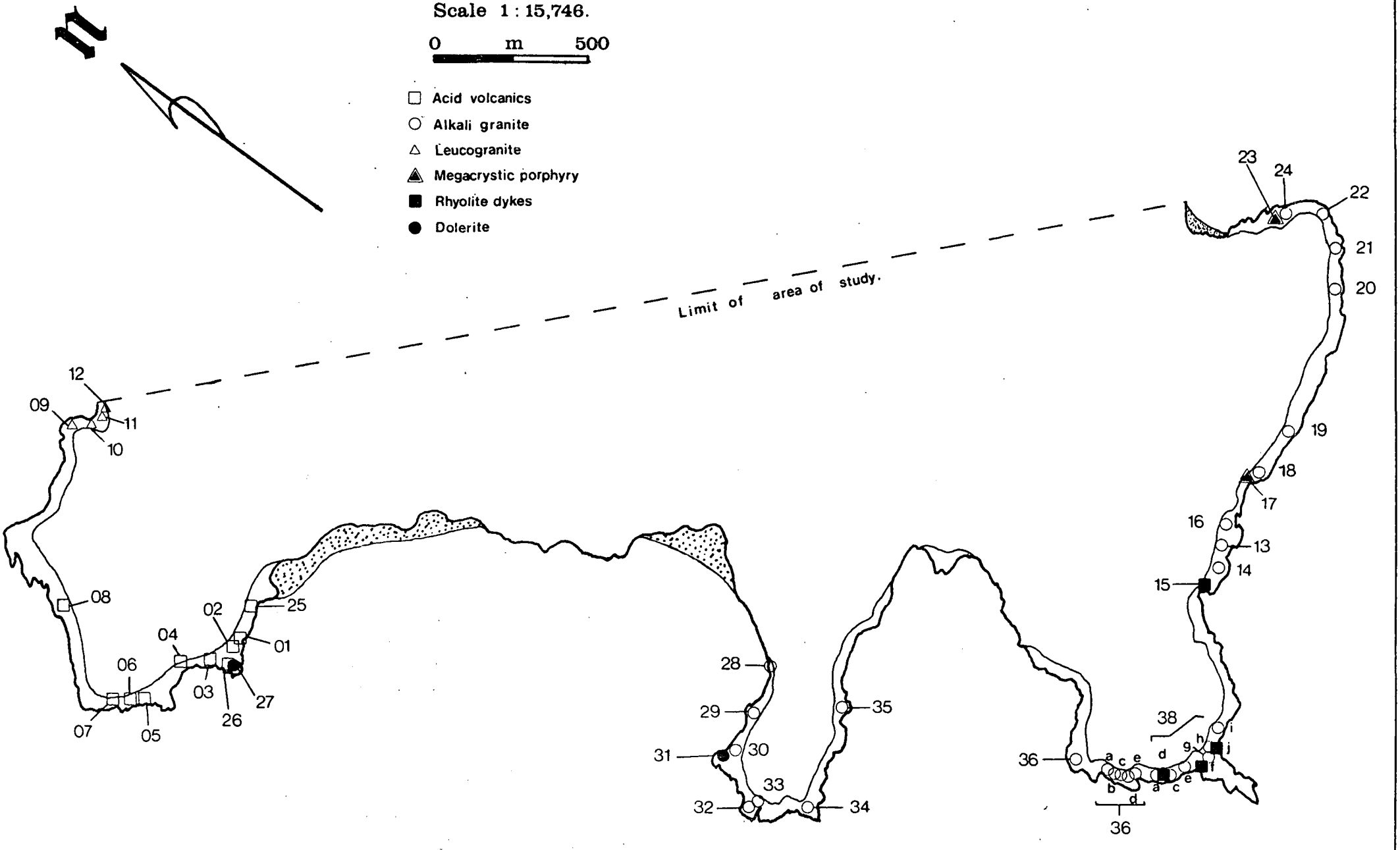

Refer to sample location map for specific rock lithology.

Appendix I.

	794/01			794/02	
794/03	794/04			794/05	
	A.V.	A.V.	Weight percentage 17 V	17 V	
SiO_2	70.38	67.57	70.25	70.80	77.78
Al_2O_3	14.68	15.85	15.06	14.60	11.92
Fe_2O_3	0.96	1.59	1.00	0.95	0.32
FeO	0.96	1.60	1.01	0.95	0.32
MnO	0.08	0.08	0.08	0.09	0.06
MgO	0.51	1.13	0.52	0.58	0.06
CaO	1.50	2.79	1.91	1.26	0.39
Na_2O	4.29	4.18	4.59	4.03	3.50
K_2O	4.48	3.05	3.66	5.03	4.96
TiO_2	0.33	0.38	0.33	0.31	0.13
P_2O_5	0.08	0.16	0.08	0.07	0.01
H_2O+	1.15	0.95	0.57	0.70	0.24
Total	99.40	99.34	99.06	99.37	99.69

Trace Elements (ppm).

Ba	1371	1459	1392	1365	138
Rb	144	147	119	174	220
Sr	266	394	287	194	47
Zr	211	192	204	200	109
Nb	12	6	11	12	16
Y	31	15	30	31	29
Ce	118	60	122	92	64
Nd	38	17	39	25	19
Ni	4	11	6	7	9
V	21	41	24	24	5
Sc	6	6	6	7	4

C.I.P.W. Norm.

Q	24.26	23.83	24.60	24.43	37.44
C	0.23	0.97	0.27	0.39	0.11
OR	26.46	18.03	21.62	29.75	29.30
AB	36.30	35.37	38.87	34.11	29.63
AN	6.94	12.82	8.95	5.80	1.86
HY EN	1.28	2.81	1.29	1.43	0.15
FS	0.59	1.16	0.63	0.63	0.22
MT	1.39	2.31	1.46	1.37	0.46
IL	0.62	0.71	0.62	0.58	0.25
AP	0.18	0.37	0.18	0.16	0.02
Total	98.25	98.39	98.49	98.67	99.46

Appendix I (cont.)

Weight percentage.

	794/06 PV	794/07 AV	794/09 Leucog	794/11 Leucog	794/12 leucogr	794/13 A.G.	794/15 Rh. Dyke
SiO_2	70.77	69.17	77.13	77.79	77.96	77.11	77.10
Al_2O_3	14.60	15.40	12.38	12.34	11.19	12.37	11.17
Fe_2O_3	0.93	1.36	0.38	0.20	0.60	0.33	0.97
FeO	0.94	1.38	0.38	0.20	0.60	0.34	0.97
MnO	0.11	0.09	0.06		0.02	0.01	0.08
MgO	0.53	1.02	0.12	0.07	0.08	0.16	0.16
CaO	1.58	3.15	0.45	0.20	0.05	0.03	0.07
Na_2O	4.39	3.88	2.74	3.80	4.25	4.29	4.47
K_2O	3.97	3.20	5.26	4.92	4.39	4.73	4.29
TiO_2	0.32	0.32	0.15	0.13	0.16	0.13	0.16
P_2O_5	0.09	0.14	0.02	0.02	0.02	0.02	0.01
H_2O+	0.63	0.70	0.67	0.29	0.30	0.16	0.18
Total	98.86	99.80	99.73	99.97	99.60	99.68	99.63

Trace Elements (ppm).

Ba	1342	1605	195	52	-	292	10
Rb	133	85	277	252	-	219	263
Sr	209	634	43	22	-	25	7
Zr	204	152	116	122	-	180	680
Nb	11	6	16	17	-	11	26
Y	30	14	27	24	-	39	105
Ce	111	63	76	40	-	76	159
Nd	30	15	21	15	-	33	56
Ni	11	9	8	8	-	8	13
V	24	41	5	6	-	4	6
Sc	7	5	4	4	-	5	8

C.I.P.W. Norm.

Q	25.80	26.00	39.84	36.41	36.86	33.71	34.96
C	0.41	0.16	1.40	0.46		0.18	
OR	23.49	18.90	31.11	29.05	25.93	27.97	25.37
AB	37.17	32.85	23.20	32.15	33.12	36.33	33.56
AN	7.25	14.71	2.09	0.86		0.02	
AC					1.73		2.79
NS					0.20		0.26
DI WO					0.05		0.12
EN					0.01		0.02
FS					0.04		0.10
HY EN	1.31	2.55	0.30	0.17	0.19	0.40	0.37
FS	0.63	1.03	0.25		0.84	0.15	1.57
MT	1.35	1.97	0.54	0.28		0.49	
IL	0.60	0.60	0.28	0.25	0.30	0.25	0.30
HM				0.00			
AP	0.21	0.32	0.05	0.05	0.05	0.05	0.02
Total	98.23	99.10	99.06	99.68	99.30	99.52	99.45

Appendix I (cont.)

Weight percentage.

	AY 794/17 MP	794/18 AG	794/19 AG	794/20 AG	794/21 AG	794/22 AG	AY 794/23 M.P.
SiO_2	68.07	78.01	78.53	77.55	78.39	78.99	69.41
Al_2O_3	14.54	11.31	11.58	11.20	11.12	10.60	14.75
Fe_2O_3	1.34	0.71	0.27	1.11	0.51	0.92	1.31
FeO	1.35	0.71	0.27	1.12	0.51	0.93	1.32
MnO	0.15	0.01		0.06	0.02	0.15	0.28
MgO	0.73	0.07	0.12	0.09	0.10	0.11	0.75
CaO	1.19	0.03	0.02	0.09	0.02	0.07	1.07
Na_2O	4.16	3.98	4.02	4.37	4.15	4.10	4.61
K_2O	6.31	4.22	4.38	3.87	4.33	3.74	4.46
TiO_2	0.54	0.16	0.15	0.13	0.15	0.16	0.50
P_2O_5	0.18	0.01	0.01	0.01	0.01	0.01	0.15
H_2O+	0.43	0.26	0.40	0.17	0.18	0.14	0.71
Total	98.98	99.47	99.77	99.78	99.49	99.93	99.34

Trace Elements (ppm).

Ba	1805	6	24	8	5	8	1762
Rb	271	197	176	182	199	205	92
Sr	214	5	8	7	3	7	242
Zr	255	581	358	634	362	586	265
Nb	8	23	12	24	14	25	9
Y	53	45	43	46	31	76	50
Ce	162	17	13	53	26	68	164
Nd	63	6	1	12	7	20	64
Ni	8	4	8	0	8	9	8
V	9	11	5	6	6	5	30
Sc	11	8	2	11	5	8	9

C.I.P.W. Norm

Q	16.73	38.35	38.15	36.71	37.77	40.24	22.08
C		0.17	0.21				0.77
OR	37.31	24.93	25.90	22.89	25.60	22.13	26.35
AB	35.22	33.67	34.05	36.05	33.08	33.65	38.98
AN	2.34	0.08	0.03				4.35
AC				0.84	1.47	0.95	
NS					0.09		
DI WO	1.01			0.16	0.01	0.12	
EN	0.66			0.03	0.00	0.02	
FS	0.28			0.15	0.01	0.10	
HY EN	1.15	0.17	0.30	0.20	0.24	0.25	1.88
FS	0.48	0.48	0.03	1.13	0.72	1.13	1.04
MT	1.94	1.02	0.40	1.19		0.86	1.90
IL	1.02	0.30	0.28	0.25	0.28	0.30	0.94
AP	0.42	0.02	0.02	0.02	0.02	0.02	0.35
Total	98.56	99.21	99.37	99.61	99.31	99.79	98.63

Appendix I (cont.)

Weight Percentage

	794/24 A.G.	794/25 A.V.	794/26 Dol.	794/27 A.V.	794/28 A.G.	794/29 A.G.	794/30 A.G.
SiO_2	78.05	66.08	47.74	70.46	77.98	78.53	78.30
Al_2O_3	10.87	16.37	16.69	15.01	11.22	11.02	11.17
Fe_2O_3	0.63	1.62	1.98	1.01	0.78	0.67	0.72
FeO	0.63	1.63	7.91	1.02	0.79	0.68	0.73
MnO	0.05	0.08	0.19	0.09	0.02	0.07	0.01
MgO	0.15	1.19	8.17	0.09	0.10	0.10	0.05
CaO	0.55	3.23	8.44	1.81	0.02	0.05	0.03
Na_2O	3.57	4.43	4.31	4.49	3.83	4.19	3.78
K_2O	4.67	3.12	2.22	4.01	4.48	4.24	4.51
TIOl	0.15	0.39	0.71	0.33	0.17	0.15	0.16
P_2O_5	0.01	0.17	0.19	0.09	0.01		0.01
H_2O+	0.54	1.00	2.69	0.69	0.24	0.29	0.41
Total	99.87	99.30	101.25	99.65	99.63	99.98	99.89

Trace Elements (ppm).

Ba	52	1466	683	1402	7	18	22
Rb	142	124	143	129	205	205	227
Sr	13	648	525	279	3	12	10
Zr	439	187	51	205	443	445	604
Nb	15	6	2	11	19	20	24
Y	56	15	12	31	49	40	32
Ce	67	74	31	40	38	8	28
Nd	32	19	8	14	4	14	4
Ni	5	7	151	7	7	8	8
V	7	40	216	94	9	10	11
Sc	6	7	30	5	7	6	6

C.I.P.W. Norm

Q		38.40	19.66		24.11	38.15	37.83	38.68
C			0.26		0.21	0.06		0.04
OR		27.63	18.43	13.11	23.71	26.47	25.04	26.66
AB		29.89	37.45	14.79	37.98	32.42	33.08	32.02
AN			14.91	19.64	8.38	0.03		0.08
NE				11.75				
AC		0.28					1.95	
NS							0.03	
DI	WO	0.93		8.75			0.10	
	EN	0.37		5.21			0.02	
	FS	0.57		3.09			0.09	
WO		0.17						
HY	EN		2.96		1.61	0.22	0.23	0.12
	FS		1.17		0.66	0.56	1.04	0.50
OL	FO			10.62				
	FA			6.95				
MT		0.77	2.35	2.86	1.47	1.13		1.05
IL		0.28	0.73	1.35	0.62	0.32	0.28	0.30
AP		0.02	0.39	0.45	0.21	0.02		0.02
Total		99.33	98.31	98.56	98.96	99.39	99.70	99.48

Appendix I (cont.)

Weight Percentages.

	794/31 Dol	794/32 AG	794/33 AG	794/34 AG	794/35 AG	794/36 AG	794/36A AG
SiO_2	47.80	77.97	77.89	77.89	77.94	77.67	77.67
Al_2O_3	17.94	11.20	11.14	11.21	11.36	11.06	11.29
Fe_2O_3	2.12	0.83	0.69	0.71	0.76	0.79	0.82
FeO	8.48	0.84	0.70	0.72	0.76	0.80	0.83
MnO	0.18	0.18	0.10	0.11	0.04	0.11	0.06
CaO	7.81	0.10	0.08	0.08	0.02	0.09	0.03
Na_2O	3.78	4.22	3.83	4.07	3.97	3.99	4.06
K_2O	0.76	4.04	4.48	4.36	4.40	4.44	4.49
TiO_2	1.09	0.15	0.15	0.14	0.15	0.15	0.15
P_2O_5	0.48	0.01	0.01	0.01	0.01	0.02	0.02
H_2O+	2.00	0.23	0.26	0.29	0.25	0.24	0.25
Total	98.73	99.91	99.36	99.69	99.72	99.46	99.76

Trace Elements (ppm).

Ba	745	5	11	3	14	2	8
Rb	31	234	213	246	232	246	251
Sr	947	4	15	8	6	10	4
Zr	65	600	570	410	603	527	563
Nb	2	23	21	18	23	20	23
Y	19	63	62	66	31	60	39
Ce	68	68	54	48	17	47	25
Nd	16	18	41	29	6	25	4
Ni	46	9	7	13	2	8	10
V	227	5	8	5	9	5	8
Sc	25	7	8	6	7	6	9

C.I.P.W. Norm.

Q		37.31	38.02	37.12	37.65	37.09	36.55
C					0.06		
OR	4.52	23.88	26.47	25.75	26.00	26.24	26.53
AB	32.01	35.14	32.37	33.39	33.59	32.19	33.09
AN	29.73				0.03		
AC		0.51	0.03	0.91		1.39	1.11
DI WO	2.46	0.18	0.14	0.14		0.13	0.00
EN	1.33	0.04	0.02	0.03		0.02	0.00
FS	1.05	0.15	0.13	0.11		0.12	0.00
HY EN	1.35	0.28	0.10	0.24	0.12	0.22	0.22
FS	1.05	0.94	0.53	0.85	0.60	1.04	1.02
OL FO	9.10						
FA	7.92						
MT	3.07	0.95	0.99	0.57	1.10	0.45	0.64
IL	2.07	0.28	0.28	0.27	0.28	0.28	0.28
AP	1.12	0.02	0.02	0.02	0.02	0.05	0.05
Total	96.73	99.68	99.11	99.40	99.47	99.22	99.51

Appendix I (cont.)

Weight Percentage.

	794/36B AG	794/36C AG	794/36D AG	794/36E AG	794/38A AG	794/38B AG	794/38C AG
SiO_2	78.88	77.62	78.34	78.18	78.60	78.23	77.89
Al_2O_3	11.20	11.24	11.23	11.10	11.17	11.10	11.24
Fe_2O_3	0.55	0.89	0.65	0.74	0.46	0.72	0.72
FeO	0.55	0.90	0.65	0.74	0.46	0.73	0.72
MnO	0.01	0.15	0.02	0.04			0.03
MgO	0.13	0.10	0.04	0.04	0.05	0.03	
CaO	0.02	0.15	0.03	0.03	0.03	0.03	0.02
Na_2O	4.07	4.14	4.22	4.31	4.03	3.97	3.99
K_2O	4.30	4.26	4.32	4.37	4.60	4.38	4.48
TiO_2	0.17	0.21	0.15	0.14	0.15	0.15	0.16
P_2O_5	0.01	0.03	0.02	0.02	0.02	0.02	0.01
H_2O+	0.20	0.22	0.17	0.22	0.25	0.23	0.26
Total	100.09	99.90	99.84	99.93	99.83	99.59	99.51

Trace Elements (ppm).

Ba	11	5	6	2	23	14	71
Rb	209	194	213	198	191	205	223
Sr	4	8	4	2	8	6	5
Zr	352	585	356	537	400	476	552
Nb	16	24	15	20	15	20	21
Y	31	75	32	44	24	41	42
Ce	24	80	30	60	36	18	63
Nd	6	44	5	16	18	4	20
Ni	4	8	7	5	8	8	0
V	5	6	6	7	8	10	4
Sc	6	6	5	6	4	5	6

C.I.P.W. Norm.

Q	38.49	36.69	37.19	37.07	37.97	38.20	37.39
C			25.55	25.83	27.18	25.88	26.47
OR	25.42	25.18	33.70	32.74	31.87	32.73	32.89
AB	33.65	34.07					
AN			1.79	2.14	1.33	0.76	0.77
AC	0.71	0.85		0.30	0.17		
DI WO	0.01	0.23	0.00	0.00	0.00	0.00	0.01
EN	0.01	0.05	0.00	0.00	0.00	0.00	
FS	0.00	0.20	0.00	0.00	0.00	0.00	0.02
HY EN	0.32	0.20	0.10	0.10	0.12	0.07	
FS	0.49	0.89	0.95	1.20	0.60	0.70	0.73
MT	0.44	0.86	0.04		0.66	0.66	0.65
IL	0.32	0.40	0.28	0.27	0.28	0.28	0.30
AP	0.02	0.07	0.05	0.05	0.05	0.05	0.02
Total	99.89	99.68	99.67	99.71	99.58	99.36	99.25

Appendix I (cont.)

Weight Percentage.

	794/38D AG	794/38E AG	794/38F AG	794/38H AG	794/38I AG
SiO_2	75.94	78.08	77.08	76.49	78.57
Al_2O_3	12.43	11.28	12.52	12.33	11.50
Fe_2O_3	0.42	0.62	0.04	0.37	0.27
FeO	0.42	0.63	0.04	0.37	0.27
MnO	0.08	0.02	0.01	0.05	0.04
MgO	0.16	0. 9	0.12	0.17	0.13
CaO	0.35	0.02	0.06	0.22	0.03
Na_2O	4.38	4.33	4.15	4.13	4.02
K_2O	4.76	4.35	4.92	4.90	4.44
TiO_2	0.16	0.16	0.16	0.15	0.16
P_2O_5	0.01	0.01	0.01	0.02	0.01
H_2O+	0.26	0.30	0.97	0.20	0.40
Total	99.36	99.87	100.07	99.39	99.85

Trace Elements (ppm).

Ba	340	6	115	101	37
Rb	177	206	198	227	200
Sr	16	6	17	14	31
Zr	173	512	171	170	417
Nb	13	20	13	14	15
Y	46	19	14	37	22
Ce	88	12	9	58	18
Nd	40	3	6	28	1
Ni	8	7	0	4	5
V	4	7	8	4	2
Sc	6	5	4	4	2

C.I.P.W. Norm.

Q	31.48	36.62	33.82	33.00	37.90
C	28.12	25.69	0.28		0.05
OR	37.05	33.80	29.09	28.96	26.25
AB	0.21		35.11	34.96	34.05
AN			0.23	0.61	0.08
AC				0.14	
NS				0.09	
DI WO		1.80		0.05	
EN		0.18	0.30	0.33	0.32
FS	0.61	0.01		0.17	0.08
HY EN	0.33	0.00		0.53	0.39
FS	0.26	0.01	0.11	0.28	0.30
MT	0.07	0.22	0.04		
IL	0.05	0.91	0.10		
HM	0.61				
RU	0.30	0.30			
AP	0.02	0.02	0.02	0.05	0.02
Total	99.11	99.57	99.10	99.19	99.45

Appendix II.

Trace Element Analysis Conditions,
Phillips X.R.F.

Element:	Ni	V
X-ray tube operating conditions	2 KW Au (50 kv/40 mA)	60 kV W vc 40 mA
Count rate:	100 sec.	2 x 40 sec.
Analytical line:	71.56°	93.49°
Background:	70.56°	91.49°
Interference:	-	TiK 94.05°
Crystal:	LiF_{220}	LiF_{220}
Collinator	Coarse	Coarse
Detector:	S	FP
Mass-absorption coefficient:	NiKx	VKx
Counting standard:	PCC-1	MDP+V
International standard:	MNT	AGV-1

S: scintillation
FP: flow proportional
VC: vacuum

Appendix II (cont.)

Trace Element Analysis Conditions,
Phillips X.R.F.

Element:	Ce	Nd
X-ray tube operating conditions:	60 kV W vc 40 mA	60 kV W vc 40 mA
Count rate:	3 x 60 sec.	3 x 60 sec.
Analytical line:	112.06°	113.15°
Background:	111.06°	114.15°
Interference:	-	-
Crystal:	LiF_{220}	LiF_{220}
Collimator:	Coarse	Coarse
Detector:	FP	FP
Mass-absorption coefficient:	LeL	NdLx
Counting standard:	G2	G2
International standard	AGV-1	AGV-1

S: scintillation
FP: flow proportional
VC: vacuum

Appendix III.

Typical Microprobe Analyses: Feldspars.

Weight percentages.

Plagioclase feldspar

	794/05		794/06	
SiO_2	67.75	69.68	68.57	67.99
TiO_2	0.00	0.00	0.03	0.00
Al_2O_3	19.04	18.77	19.72	19.29
Cr_2O_3	0.00	0.02	0.02	0.09
FeO	0.12	0.01	0.03	0.10
MnO	0.02	0.00	0.00	0.00
MgO	0.03	0.00	0.02	0.01
CaO	0.50	0.10	0.32	0.41
Na_2O	11.30	11.60	11.00	11.07
H_2O	0.39	0.11	0.42	0.46
Total	99.13	100.29	100.13	99.42

Alkali feldspar

	794/05		794/06	
SiO_2	65.60	65.90	65.21	65.38
TiO_2	0.00	0.00	0.00	0.00
Al_2O_3	17.93	17.59	17.83	17.69
Cr_2O_3	0.00	0.00	0.00	0.03
FeO	0.00	0.00	0.03	0.04
MnO	0.01	0.00	0.00	0.02
MgO	0.00	0.00	0.00	0.00
CaO	0.13	0.00	0.00	0.12
Na_2O	2.89	0.64	0.33	2.98
H_2O	12.73	15.94	16.08	12.39
Total	99.19	100.08	99.48	98.65

Appendix III (cont.)

Microprobe Analyses: Feldspars.
Plagioclase feldspar.

		794/21	794.28	794.11	794/36
SiO_2	70.34	70.48	68.50	70.72	71.58
TiO_2	0.00	0.00	0.001	0.00	0.00
Al_2O_3	17.87	17.86	18.02	20.17	19.23
Cr_2O_3	0.00	0.00	0.03	0.00	0.00
FeO	0.56	0.69	0.30	0.03	0.08
MnO	0.02	0.00	0.05	0.00	0.00
MgO	0.00	0.00	0.001	0.01	0.00
CaO	0.00	0.00	0.00	0.76	0.00
Na_2O	11.63	11.60	11.56	8.26	10.80
K_2O	0.05	0.10	0.09	0.07	0.10
Total	100.47	100.73	98.57	100.02	101.99

Alkali Feldspar.

					794/36
SiO_2	65.70	65.08	66.85	67.63	65.34
TiO_2	0.02	0.02	0.00	0.00	0.00
Al_2O_3	17.62	17.35	18.54	18.27	17.08
Cr_2O_3	0.06	0.00	0.02	0.00	0.02
FeO	0.11	0.27	0.35	0.04	0.35
MnO	0.00	0.00	0.00	0.03	0.00
MgO	0.00	0.00	0.07	0.00	0.00
CaO	0.00	0.01	0.01	0.00	0.00
Na_2O	0.23	0.22	5.01	0.16	0.32
K_2O	16.49	16.71	8.98	16.56	16.34
Total	100.23	99.66	99.83	101.69	99.45

Appendix IV.

Brief thin section descriptions of a representative selection of rocks from Saint Francis Island.

794/01: Fractured and subrounded quartz and fledspar phenocrysts 1-3 mm diameter in a felsophyric to orthophyric groundmass. 25% phencrysts of which 20% albite, 30% quartz and 50% orthoclase. Minor chlorite and chloritized biotite as intersitial platy aggregates. Minor veinlets of carbonate and epidote.
Rhyodacite crystal tuff.

794/02: Subhedral plagioclase and quartz phenocrysts 0.5-2mm diameter in a felsophyric groundmass. 20% phenocrysts of which 80% albite, 20% quartz. Alteration consists of sericitization of feldspar grains and chloritization of biotite grains with minor carbonate.
Dacite cystal tuff.

794/05: Hypocrystalline orthophyric with euhedral quartz phenocrysts 0.5-1mm diameter often being the core of spherulites 20-25 mm diameter consisting of radiating fiberous orthoclase in an orthophyric groundmass. Quartz 20%, orthoclase (with perthitic texcture) 70%, albite 10%.
Rhyolite crystal tuff.

794/06: Apparent contact between two acid flows. One side is a hypocrystalline porphyry consisting of subhedral to subrounded quartz and feldspar phenocrysts 1-2 mm diameter in a granular orthophyric groundmass. Of the 15% phenocrysts, quartz 15%, orthoclase 50%, albite 35%. Other side has 15% phenocrysts 1-3 mm diameter consisting of 50% albite, 40% orthoclase, 10% quartz in a felsophyric groundmass. Sericitization of feldspars, chloritization of biotite with minor magnetite and epidote.
Rhyodacite crystal tuff.

794/07: Sericitized orthoclase phenocrysts (15%) 1-2 mm diameter in a felted felsophyric groundmass of alkali feldspar and plagioclase. Minor interstitial chlorite, chloritized biotite, carbonate and epidote.
Dacite crystal tuff.

794/08: Contact between two acid flows. One side consists of 7% phenocrysts 0.2 - 0.5 mm diameter of quartz (80%) and albite (20%) in an orthophyric groundmass. Minor orthoclase with slightly sericite

alteration. Minor carbonate, chlorite and magnetite. Other side has 30% phenocrysts (3 mm diameter for feldspars, 1-2 mm diameter for quartz) of which 60% orthoclase, 20% plagioclase, 20% quartz. Epidote with poikolitic zircons occur with chloritized and carbonitized biotite.

Rhyolite - rhyodacite porphyry crystal tuff.

794/11: Holocrystalline hypidiomorphic granular quartz-feldspar granite. Grains are 1-2 mm diameter consisting of 30% quartz, 20% albite and 50% orthoclase with perthitic texture. Quartz grains are enhedral with undulose extinction and are intergrown with alkali felspar developing graphic texture. Minor sericitization of feldspar with interstitial carbonate and magnetite.

Leucogranite.

794/17: Euhedral and slightly rounded megacrysts 5 mm diameter of orthoclase and microcline (30%) with smaller phenocrysts of plagioclase in an orthophyric or vitrophyric groundmass. Minor interstitial mafics consisting of chlorite, chloritized biotite and magnetite. Minor sericitization of feldspars. Groundmass shows lineated flow texture around phenocrysts.

Megacrystic dacite porphyry.

794/18: Holocrystalline quartz - feldspar porphyry with euhedral, subrounded quartz and perthitic orthoclase grains 1- 3 mm diameter (20%) in a coarse groundmass of quartz, alkali feldspar and plagioclase graphically intergrown. Myremekitic texture noted around some feldspar phenocrysts. Minor intersitial haematite and magnetite.

Alkali granite porphyry.

794/21 Holocrystalline hypidiomorphic granular with abundant quartz-feldspar graphic intergrowths. Orthoclase (60%), quartz (40%) with minor quantities of plagioclase and aegirine.

Alkali granite.

794/24: Intratelluric phenocrysts of alkali feldspar 1-2 mm diameter (50%), plagioclase 0.5-1mm diameter (25%) and quartz (25%) in an orthophyric groundmass which shows some trachytic flow banding. Minor magnetite, zircon with slightly sericitized feldspars and chlorite - epidote veining.

Rhyolite lithic tuff.

794/25: An aggregate of megacrysts 5 mm diameter of perthitic orthoclase and albite accompanied by albite, orthoclase and quartz grains 1 mm diameter in a felsophyric groundmass. Minor biotite and chlorite. Quartz 15%, alkali feldspar 55% and plagioclase 30%.
Rhyodacite.

794/26: Epidote grains 0.5 mm in diameter with hornblende in a felted ophitic groundmass of plagioclase. Hornblende 30%, epidote 20% and plagioclase 50%.
Dolerite.

794/28: Phenocrysts 3-4 mm diameter (10%) of quartz (60%) and partially myrmekitic orthoclase (40%) in a hypidiomorphic granular groundmass of feldspar and quartz of which 10% plagioclase, 50% quartz and 40% alkalifeldspar. Minor aegirine and intersitial magnetite and haematite.
Porphyritic alkali granite.

794/32: 10% phenocrysts of quartz and alkali feldspar (perthitic orthoclase) 2 mm diameter in a hypidiomorphic granular groundmass 0.5 - 1.0 mm diameter of 50% quartz, 40% alkali feldspar and 10% plagioclase. Minor interstitial aggregates of epidote (?) and zircon.
Porphyritic alkali granite.

794/36: Cumulophyric porphyry with 30% phenocrysts 2-3 mm diameter of 60% perthitic orthoclase and 40% quartz. Groundmass consists of hypidiomorphic granular grains 0.5 - 1 mm diameter of 20% quartz, 60% alkali feldspar and 20% plagioclase with minor interstitial carbonate and haematite.
Porphyritic alkali granite.

794/38A: Hypidiomorphic granular holocrystalline granite with occasional 3 mm diameter phenocrysts of orthoclase. 1 - 2 mm diameter grains of 15% plagioclase (albite), 30% quartz and 55% alkali feldspar, some of which displaying pethitic texture and graphically intergrown with quartz. Minor euhedral grains 1 - 2 mm diameter of epidote.
Alkali granite.

794/38C: Hypidiomorphic granular with grains 0.8 mm diameter consisting of 20% albite, 40% quartz and 40% alkali feldspar which display extensive graphic intergrowth. Minor interstitial magnetite and aegirine.
Alkali granite.

794/38F: Hypidiomorphic granular holocrystalline with abundant radiating alkali feldspar spherulites and quartz - alkali feldspar graphic intergrowths. Grains 0.5 - 1.0 mm in diameter with 20% quartz, 10% plagioclase and 70% alkali feldspar. Mafics consist of minor interstitial biotite.
Rhyolite dyke.

794/38I: Megacrysts of glomerophyric quartz and alkali feldspar 3 - 5 mm in diamter (40%) with lesser plagioclase in a felsite groundmass of graphically intergrown quartz and alkali feldspar. Minor interstitial carbonate and aegirine.
Porphyritic alkali granite.

794/38J: Euhedral and slightly rounded phenocrysts of quartz and alkali feldspar 2 mm in diameter consisting of 10% of the rock. Groundmass consists of radial spherulites of alkali feldspar and graphically intergrown quartz and alkali feldspar. Minor magnetite and interstitial haematite.
Rhyolite dyke.

Appendix V.

Analytical Procedure: Geochemistry.

Whole-rock geochemical analysis was initiated by first assuring that the least weathered rock was used. The sample was then crushed and pulverized by means of a jaw crusher and carbon grinding mill respectively. Approximately five grams of the resultant powder was then measured into silica crucibles and ignited at 950^{o}C for at least fourteen hours. The difference in weight thus defined the quantity lost on ignition.

0.2800 g of ignited sample was then carefully combined with 1.5000 g of flux and 0.0200 g of NaOH and was fused into discs by P. McDuie and analyses on the Siemens S.R.S. mass spectrometer by J. Stanley for all major oxides excluding Na_2O. Na_2O was measured by digesting approximately 0.3000 g of ignited rock powder in a solution of H_2SO_4 and HF which was then made to an appropriate volume with H_2SO_4 and analysed using the Corning EEL Flame Photometer.

Trace element data for Ni, V, Ce and Nd were accomplished by the analysis of pressed rock powder pellets on the Phillips PW 1540 X-ray spectrometer. Operating conditions for the various elements can be found in Appendix II. Further analyses of the pressed pellets on the Siemens S.R.S. were undertaken to determine Ba, Rb, Sr, Y, Zr, Sc and Nb contents.

Rare earth element concentrations for samples 06, 38I, were determined by first digesting a measured amount of rock powder in acids plus Spike B solution, which has a known isotope ratio for analyses enriched in light rare earth elements. The entire solution was then passed through two cation exchange colums in order to concentrate and separate heavy rare earth elements, middle rare earth elements and Ce. Samples are then loaded onto Re triple filament bead and analysed in the Thompson-CSF mass spectrometer by Dr. J. Foden.